Rethinking the role of transport and photochemistry in regional ozone pollution: Insights from ozone mass and concentration budgets

Kun Qu[1,1], Xuesong Wang[2,2], Xuhui Cai[3,3], Yu Yan[4,4], Xipeng Jin[3,3], Mihalis Vrekoussis[5,5], Jin Shen[6,6], Teng Xiao[3,3], Limin Zeng[7,7], and Yuanhang Zhang[8,8]

[1]Peking Univeristy; University of Bremen
[2]College of Environmental Sciences and Engineering
[3]Peking University
[4]Peking university
[5]Institute of Environmental Physics, University of Bremen
[6]Guangdong Environmental Monitoring Center
[7]College of Environmental Sciences and Engineering, Peking University
[8]State Key Lab

December 7, 2022

Abstract

Understanding the role of transport and photochemistry is essential to alleviate ambient ozone pollution. However, ozone budget and source apportionment studies often report conflicting conclusions — Local photochemistry is the main cause of ozone pollution based on the analyses of the former, while contrary, non-local ozone transported to the region accounts for the majority in the latter results. In order to explore its potential causes, we calculated the contributions of both processes to the variations of mean ozone concentration and total ozone mass (the corresponding budgets are noted as ozone concentration and mass budget, respectively) within the atmospheric boundary layer (ABL) of the Pearl River Delta (PRD), China, based on the modelling results of WRF-CMAQ. Quantified results show that photochemistry drives the rapid increase of ozone concentrations in the daytime, whereas transport, especially the vertical exchange near the ABL top, controls the ozone mass budget. The changes in transport contributions in ozone budgets indicate the influences of the ABL diurnal cycle and regional wind fields, including prevailing winds and local circulations (sea breezes), on regional ozone pollution. Though transport in our simulations had a relatively limited effect on ozone concentration, its high contribution to ozone mass increase in the morning determined that most ozone in the PRD emanated from the outer regions. Consequently, the role of transport and photochemistry in ozone pollution may differ, depending on which of the two budgets is concerned. For future studies targeting ozone and other pollutants with moderately long atmospheric lifetimes, we suggest that attention should be paid to budget-type selections.

Rethinking the role of transport and photochemistry in regional ozone pollution: Insights from ozone concentration and mass budgets

Kun Qu[1,2,3], Xuesong Wang[1,2], Xuhui Cai[1,2], Yu Yan[1,2], Xipeng Jin[1,2], Mihalis Vrekoussis[3,4,5], Jin Shen[6], Teng Xiao[1,2], Limin Zeng[1,2], and Yuanhang Zhang[1,2,7,8]

[1]State Key Joint Laboratory of Environmental Simulation and Pollution Control, College of Environmental Sciences and Engineering, Peking University, Beijing 100871, China
[2]International Joint Laboratory for Regional Pollution Control, Ministry of Education, Beijing, 100816, China
[3]Laboratory for Modeling and Observation of the Earth System (LAMOS), Institute of Environmental Physics (IUP), University of Bremen, Bremen, Germany
[4]Center of Marine Environmental Sciences (MARUM), University of Bremen, Germany
[5]Climate and Atmosphere Research Center (CARE-C), The Cyprus Institute, Cyprus
[6]State Key Laboratory of Regional Air Quality Monitoring, Guangdong Key Laboratory of Secondary Air Pollution Research, Guangdong Environmental Monitoring Center, Guangzhou 510308, China
[7]Beijing Innovation Center for Engineering Science and Advanced Technology, Peking University, Beijing 100871, China
[8]CAS Center for Excellence in Regional Atmospheric Environment, Chinese Academy of Sciences, Xiamen 361021, China

Correspondence to: Xuesong Wang (xswang@pku.edu.cn) and Yuanhang Zhang (yhzhang@pku.edu.cn)

Abstract. Understanding the role of transport and photochemistry is essential to alleviate ambient ozone pollution. However, ozone budget and source apportionment studies often report conflicting conclusions — Local photochemistry is the main cause of ozone pollution based on the analyses of the former, while contrary, non-local ozone transported to the region accounts for the majority in the latter results. In order to explore its potential causes, we calculated the contributions of both processes to the variations of mean ozone concentration and total ozone mass (the corresponding budgets are noted as ozone concentration and mass budget, respectively) within the atmospheric boundary layer (ABL) of the Pearl River Delta (PRD), China, based on the modelling results of WRF-CMAQ. Quantified results show that photochemistry drives the rapid increase of ozone concentrations in the daytime, whereas transport, especially the vertical exchange near the ABL top, controls the ozone mass budget. The changes in transport contributions in ozone budgets indicate the influences of the ABL diurnal cycle and regional wind fields, including prevailing winds and local circulations (sea breezes), on regional ozone pollution. Though transport in our simulations had a relatively limited effect on ozone concentration, its high contribution to ozone mass increase in the morning determined that most ozone in the PRD emanated from the outer regions. Consequently, the role of transport and photochemistry in ozone pollution may differ, depending on which of the two budgets is concerned. For future studies targeting ozone and other pollutants with moderately long atmospheric lifetimes, we suggest that attention should be paid to budget-type selections.

1 Introduction

Since first recognized in the Los Angeles smog, ambient ozone (O_3) pollution has been a problem for many highly populated urban regions around the globe (Fishman et al., 2003; Schultz et al., 2017; Fleming et al., 2018; Fowler et al., 2020). Exposure to O_3 threatens human health, crop yields and ecosystems, and results in increased mortality and economic losses (Mills et al., 2013; Ainsworth, 2017; Zhang et al., 2019). In addition, O_3 contributes to global warming not only directly as a greenhouse gas, but also indirectly by damaging plants and suppressing land carbon sinks (Sitch et al., 2007; Naik et al., 2021). Considering the above detrimental effects, efforts to reduce ambient O_3 pollution in polluted urban regions are keenly required.

Understanding O_3 processes in the atmosphere is an essential prerequisite to finding effective regional O_3 control strategies. Generally, high O_3 concentrations within a region are attributed to daytime photochemical production from O_3 precursors, i.e. NO_x (= NO + NO_2) and volatile organic compounds (VOCs), under the sunlight. However, since O_3 has a moderately long atmospheric lifetime (20-30 days; Stevenson et al., 2006; Bates and Jacob, 2019), the influence of dynamic processes on regional-level O_3 pollution is likely to be important as well (Vilà-Guerau de Arellano et al., 2015). This can be shown by the following two aspects. Firstly, O_3 is well mixed in the daytime convective atmospheric boundary layer (ABL), especially during severe O_3 pollution (Zhao et al., 2019; Tang et al., 2021). Due to ABL mixing, O_3 precursors emitted by near-ground sources are brought upwards to the upper ABL, where O_3 is more rapidly produced; afterwards, O_3 is transported downwards to the ground (Tang et al., 2017). Therefore, to alleviate near-ground O_3 pollution, the goal should be to reduce the overall O_3 level within the ABL — rather than only near the ground — based on the quantified influence of various O_3 processes throughout the ABL. Secondly, transport, including horizontal transport (mainly advection) and vertical exchange near the ABL top, may considerably contribute to regional O_3 pollution. More specially, through the vertical exchange in the morning, O_3 in the residual layer and/or free atmosphere is entrained into the ABL, leading to the rapid increase of O_3 concentration after sunrise (Kaser et al., 2017; Hu et al., 2018; Zhao et al., 2019). Transported O_3 may be derived from local sources, or transported from other regions, continents and even stratosphere under the combined effect of meso-, synoptic-, large- and global-scale atmospheric movements (Massagué et al., 2019). In addition, O_3 precursors may also be transported into the region and involved in O_3 production. These dynamic processes make the causes of regional O_3 pollution more complicated than normally realized.

In previous studies, the O_3 budget was often conducted to quantify the contributions of various chemical and transport processes to the variations of O_3 concentrations. For the mean O_3 concentration within the ABL ($\langle c_{O_3} \rangle$), its budget can be represented as in Lenschow et al. (1981), Janssen and Pozzer (2015) and Vilà-Guerau de Arellano et al. (2015):

$$\frac{\partial \langle c_{O_3} \rangle}{\partial t} = -\left(\bar{u} \frac{\partial \langle c_{O_3} \rangle}{\partial x} + \bar{v} \frac{\partial \langle c_{O_3} \rangle}{\partial y} \right) - \frac{\partial \overline{c_{O_3}' w'}}{\partial z} + S(O_3) \quad (1)$$

where u, v and w indicate wind speeds in the x-, y- and z-direction, respectively. Three items on the right side of Eq. (1) separately describe the contributions of 1) horizontal transport (advection), 2) vertical exchange near the ABL top, 3) gas-phase chemistry, dry deposition and other processes (the term $S(O_3)$ indicates their net contributions). Reported O_3 budget based on ground-based measurements (Su et al., 2018; Tan et al., 2018; Tan et al., 2019; Yu et al., 2020), aircraft-based mobile observations (Lenschow et al., 1981; Trousdell et al., 2016; Trousdell et al., 2019) and Process Analysis (PA) or alike modules in chemical transport models (CTMs) (Hou et al., 2014; Li et al., 2021a; Yan et al., 2021) often suggest that O_3 production through local photochemistry drives the noon-time increase of O_3 concentration, whereas transport reduces O_3 concentration over the same period. O_3 precursors are likely to be mainly derived from local emissions due to their relatively short lifetimes. Thus, according to these photochemistry-dominated O_3 budget results, local emission reduction seems more efficient in alleviating ambient O_3 pollution.

As an important characteristic of O_3, O_3 source indicates from which regions and/or emission sectors O_3 originates, of which the results can support effective air pollution control (Clappier et al., 2017; Thunis et al., 2019). The source apportionment of ambient O_3 often suggested that most O_3 emanated from non-local sources, including the global background and emissions outside the targeted regions (Guo et al., 2018; Pay et al., 2019; Liu et al., 2020). The mixing ratios of background O_3 in various regions of the world are mostly within the range of 30-50 ppb (Reid et al., 2008), high enough to ensure the dominance of non-local sources for O_3 pollution in less polluted regions. Since this part of O_3 is less likely to be controlled, the influence of O_3 and/or precursors transport from the upwind metropolitan regions has received much attention (Lelieveld et al., 2009; Boian and Andrade, 2012; Massagué et al., 2019). For regions where upwind sources notably contribute to O_3, focusing more on emission reductions on a larger scale rather than only reducing local emissions is needed to effectively control O_3 pollution. One successful example is the establishment of the "Ozone Transport Region" in the north-eastern US by the US Environmental Protection Agency, which promoted collaborative emission reductions among states to address inter-state O_3 transport (Novel, 1992). In China, O_3 pollution was overall more severe than in other countries recently (Lu et al., 2018). Since high pollutant emissions are widely distributed in East China, the so-called "gigacity" (Kulmala et al., 2021), upwind emissions often contribute more to O_3 pollution in the major city clusters compared to local emissions, as suggested by O_3 source studies in China (Liu et al., 2020). Therefore, transport seems to play a more important role in ambient O_3 pollution here as well, and the efforts of joint prevention and control among regions to reduce O_3 levels are necessary (Li et al., 2021b). Apparently, insights from O_3 source apportionment differ from the conclusions based on the O_3 budgets.

Simulations by Eulerian CTMs are capable of reproducing O_3 processes within the ABL. However, since the contribution of vertical exchange near the ABL top is not specifically quantified in normally used ABL parameterizations, it cannot be directly provided by the PA module but requires additional calculations (Kaser et al., 2017). Thus O_3 budget within the ABL on the hourly scale is seldom reported based on CTMs results. In this study, we constructed the post-processing tool

flux_4d_cal to quantify the contributions of O_3 processes, including gas-phase chemistry, horizontal transport and vertical exchange near the ABL top, in the O_3 budget within the ABL of the targeted region. The calculations were conducted based on the simulation results from the Weather Research and Forecasting (WRF) and Community Multiscale Air Quality (CMAQ) models, of which the details are briefly introduced in Sect. 2. To explore the reasons behind the contradictory views on the role of transport and photochemistry in regional ozone pollution between the O_3 budget in Eq. (1) and O_3 source apportionment, the other type of O_3 budget, the O_3 mass budget, was introduced by this tool. It aims to identify the contributions of O_3 processes to the variation of total O_3 mass within the ABL (m_{O_3}) and is written as:

$$\frac{\partial m_{O_3}}{\partial t} = -\left(\bar{u}s_x\langle c_{O_3}\rangle + \bar{v}s_y\langle c_{O_3}\rangle\right) - \overline{c_{O_3}'w'}s_z + S(O_3)V \quad (2)$$

where s_x, s_y, s_z are the areas of the interfaces in the x-, y- and z-direction, respectively, and V is the volume of the ABL column. Regional-level O_3 mass budget can be applied to illustrate better the changes in regional O_3 sources and their influencing factors (more in-detail discussions are given in Sect. 2.4). The O_3 budget shown in Eq. (1) is hereinafter re-defined as the O_3 concentration budget, which focuses on the contributions of O_3 processes to the variation of ABL-mean O_3 concentration. Moreover, based on the O_3 mass budgets in the sensitivity scenarios that zeroes out emissions in specific regions, the regional source of O_3 mass change contributed by different processes can also be identified. The Pearl River Delta (PRD) region, a city cluster located on the southeast coast of China and exposed to severe O_3 pollution in summer and autumn (Gao et al., 2018), was selected as the targeted region in this study. The quantified results of O_3 concentration and mass budgets in the PRD illustrated the complex effects of O_3 processes, especially transport, on regional O_3 pollution, and revealed that the distinct views on the role of photochemistry and transport are possibly linked to the differences between two O_3 budgets.

2 Methodology: O_3 budget calculations and model setup

2.1 Processes in O_3 budgets

Figure 1 displays all processes considered in the calculation of O_3 budgets as well as the distributions of the PRD grids (lower-left panel; defined as the grids within the PRD), which include the border grids (defined as the PRD grids adjacent to the outer regions) and non-border grids.

Horizontal transport through the borders of the PRD in four directions and vertical exchange near the ABL top are the transport processes concerned in this study. For the latter, its contribution in the O_3 concentration budget (the second item on the right side of Eq. (1)) is quantified by Sinclair et al. (2010) and Jin et al. (2021):

$$-\frac{\partial\overline{c_{O_3}'w'}}{\partial z} = -\frac{\Delta c_{O_3}}{H}\frac{\partial H}{\partial t} - \frac{\Delta c_{O_3}}{H}\left(u_h\frac{\partial H}{\partial x} + v_h\frac{\partial H}{\partial y} - w_h\right) \quad (3)$$

where H is the ABL height; Δc_{O_3} is the difference between O_3 concentrations above and within the ABL; u_h, v_h and w_h are the ABL-top wind speeds in the x, y and z-direction, respectively. Items on the right side of Eq. (3) suggested that the occurrence of vertical exchange is attributed to 1) the temporal changes of ABL heights and 2) large-scale air motion (advection) perpendicular to the ABL top and its slope. Their contributions can be identified in the O_3 mass budget as well, of which the details are introduced in Sect 2.2. Hereafter, vertical exchanges due to the above two processes are marked as ABLex-H and ABLex-M, respectively. The contributions of all transport processes were quantified using meteorological parameters and O_3 concentrations modelled by WRF-CMAQ. The basic calculations of the above contributions in the O_3 concentration and mass budgets are separately introduced in the following two sections, and details about the calculation process are presented in Text S1.

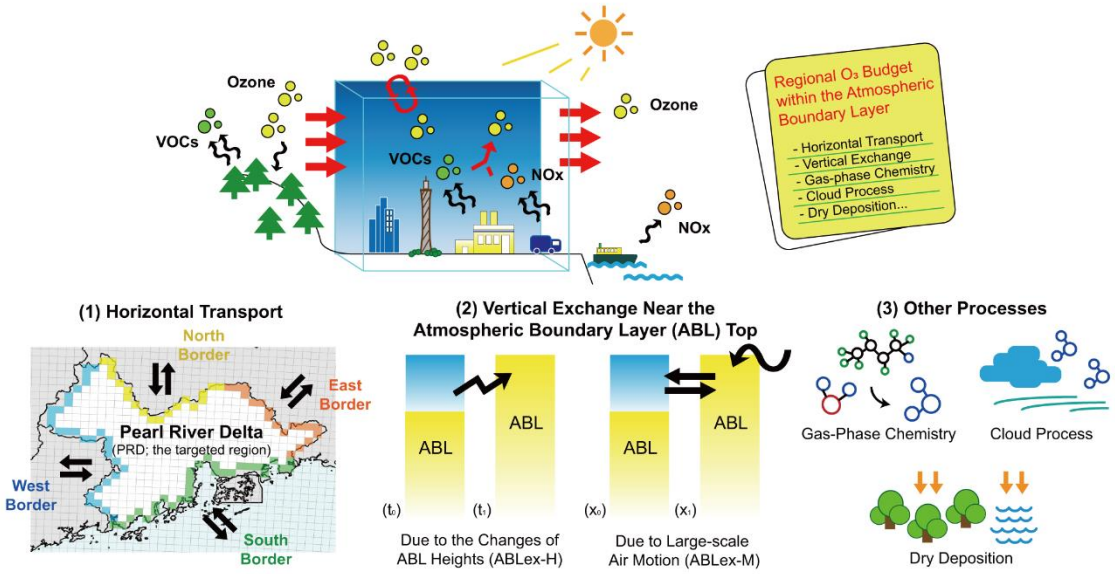

Figure 1. Schematic illustration of regional O_3 budgets (the upper panel) and processes considered (the lower panel): (1) Horizontal transport through the borders of the Pearl River Delta (PRD) in four directions (the distributions of the PRD grids are also shown: yellow, green, blue, orange for the north, south, west and east border grids, respectively, and white for the non-border grids); (2) Vertical exchange near the atmospheric boundary layer (ABL) top, including the process due to the changes of ABL heights (ABLex-H) and large-scale air motion (ABLex-M); (3) Other processes, including gas-phase chemistry, cloud process and dry deposition in this study.

Other processes in O_3 budgets include gas-phase chemistry (including daytime photochemical O_3 production and O_3 titration by NO), cloud process (including below and in-cloud mixing, aqueous-phase chemistry, wet deposition; Liu et al., 2011) and dry deposition. Their contributions are calculated based on the output of the PA module in CMAQ (for a more detailed description of calculations, see Text S1). Since diffusion near the boundaries and top of the region is expected to have a minor influence on the variation of O_3 concentration and mass, we did not involve this process in the quantifications.

2.2 Transport contributions in the O_3 mass budget

The method by Yang et al. (2012) and Chang et al. (2018) was applied to quantify the contributions of horizontal transport in the O_3 mass budget. For instance, the contribution of the advection through the west/east interface of a grid cell column within the ABL to total O_3 mass (F_{htrans}) in the column during the time interval dt is calculated as:

$$F_{htrans} = \int_0^H c_{O_3} uL \, dz \, dt \tag{4}$$

where L is the width of the grid cell (equal to the horizontal resolution of the model); dz is the height of vertical layers. For advection through the north/south interface, the calculation is similar to Eq. (4), except for using v instead of u. F_{htrans} values through every interface between one type of border and the outer region were summed up as the net contribution of horizontal transport through that border in the O_3 mass budget.

Following Sinclair et al. (2010) and Jin et al. (2021), the contribution of vertical exchange near the ABL top to O_3 mass (F_{ABLex}) during the time interval dt can be expressed as:

$$F_{ABLex} = F_{ABLex-H} + F_{ABLex-M} = c_{O_3\_h} \frac{\partial H}{\partial t} L^2 dt + c_{O_3\_h} \left(u_h \frac{\partial H}{\partial x} + v_h \frac{\partial H}{\partial y} - w_h \right) L^2 dt \tag{5}$$

where $c_{O_3\_h}$ is the O_3 concentration at the ABL top. Two terms on the right-most side of Eq. (5) separately describe the contributions of ABLex-H and ABLex-M (denoted separately as $F_{ABLex-H}$ and $F_{ABLex-M}$). F_{ABLex} values in all the PRD grids were summed up as the net contribution of vertical exchange near the ABL top in the O_3 mass budget.

2.3 Transport contributions in the O_3 concentration budget

For one or limited grid columns, it is possible to directly use Eq. (1) to quantify the O_3 concentration budget based on CTMs results. But for the ABL of the PRD, which comprises over 260 grid columns, such calculations could easily become over-complicated. Therefore, a different approach was applied to calculate the regional-level O_3 concentration budget.

Suppose that air parcels with a total volume of dV are transported into the ABL of the PRD (its original volume is V) during the time interval dt. For horizontal transport, the variation of $\langle c_{O_3} \rangle$ under its influence ($d\langle c_{O_3} \rangle_{htrans}$) can be written as:

$$d\langle c_{O_3} \rangle_{htrans} = \frac{F_{htrans} + \langle c_{O_3} \rangle (V - dV)}{V} - \langle c_{O_3} \rangle = \frac{F_{htrans} - \langle c_{O_3} \rangle \, dV}{V} \tag{6}$$

Since ABLex-M is also an advection process, its contribution in the O_3 concentration budget ($d\langle c_{O_3} \rangle_{ABLex-M}$) can be quantified using a similar formula, except for using $F_{ABLex-M}$ instead of F_{htrans}.

Through ABLex-H, air parcels in the residual layer and/or free atmosphere are merged into (or segmented out of) the ABL. Thus, the variation of $\langle c_{O_3} \rangle$ under its influence ($d\langle c_{O_3} \rangle_{ABLex-H}$) is expressed as:

$$d\langle c_{O_3} \rangle_{ABLex-H} = \frac{F_{ABLex-H} + \langle c_{O_3} \rangle V}{V + dV} - \langle c_{O_3} \rangle = \frac{F_{ABLex-H} - \langle c_{O_3} \rangle \, dV}{V + dV} \quad (7)$$

If the targeted region was small enough, Eqs. (6) and (7) would have the same forms as the corresponding items in Eq. (1), confirming the applicability of the above calculations (for details, see Text S2). All variables in Eqs. (6) and (7) can be quantified by the post-processing tool, making the method suitable for calculating the regional-scale O_3 concentration budget.

However, due to the prominent diurnal cycle of ABL, V in Eqs. (6) and (7) may change notably within an hour, leading to bias in the hourly estimations of $d\langle c_{O_3} \rangle_{htrans}$, $d\langle c_{O_3} \rangle_{ABLex-H}$ and $d\langle c_{O_3} \rangle_{ABLex-M}$ when using V at the start and end of the hour. In order to reduce this potential bias, we designed two calculation paths (Fig. S1):

- O_3 mass change → ABL volume change
- ABL volume change → O_3 mass change

where only O_3 mass or ABL volume changes in each calculation step. The contribution of ABLex-H can be decomposed into two parts: ABL volume change due to ABL development (collapse) leads to lower (higher) O_3 concentration, and O_3 transported into (out of) the ABL through ABLex-H leads to O_3 increase (decrease). These contributions are quantified separately in the ABL volume and O_3 mass change step. The contributions of other processes are quantified only in the O_3 mass change step. For one process, its contribution to the variation of O_3 concentration is calculated through both paths, and the mean value of two results serves as an estimation close to its real contribution in the O_3 concentration budget.

2.4 Difference between two O_3 budgets

Suppose that the mean O_3 concentration in the transported air parcels is $\langle c_{O_3} \rangle_{trans}$. For horizontal transport, its contributions in the O_3 mass and concentration budgets can be separately written as:

$$F_{htrans} = \langle c_{O_3} \rangle_{trans} \, dV \quad (8)$$

$$d\langle c_{O_3} \rangle_{htrans} = \frac{dV}{V}\left(\langle c_{O_3} \rangle_{trans} - \langle c_{O_3} \rangle\right) \quad (9)$$

Apparently, F_{htrans} is related to the O_3 concentrations in the transported air parcels, but not to those in the targeted region. It indicates how much O_3 is transported into or out of the region. Whether it is positive or negative only depends on the direction of transport — O_3 being transported into (out of) the region leads to the increase (decrease) of O_3 mass, which corresponds to a positive (negative) contribution in the O_3 mass budget. In contrast, $d\langle c_{O_3} \rangle_{htrans}$ quantifies how much horizontal transport alters regional-mean O_3 levels. As shown in Eq. (9), it is linked to the difference between O_3 concentrations in the transported air parcels and the targeted region. O_3 being transported into (out of) the region does not

necessarily result in a higher (lower) O_3 concentration. For instance, when clean air parcels with relatively low O_3 levels are transported into the region, they dilute O_3 pollution and reduce O_3 concentration ($d\langle c_{O_3}\rangle_{htrans} < 0$). These effects are the same for ABLex-H and ABLex-M, also showing the above difference between the two O_3 budgets.

To understand the influence of various processes on O_3 sources, it is required to identify the sources of "new O_3" into the region and "disappeared O_3" out of the region contributed by processes, rather than how these processes lead to the variations of O_3 concentration. According to the above discussions, the O_3 mass budget is suitable to explain how transport and photochemistry determine the regional sources of O_3 in this study.

2.5 Model setup and validation

The O_3 concentration and mass budgets within the ABL of the PRD were calculated based on the WRF-CMAQ modelling results by Qu et al. (2021). In the models, two nested domains with the resolution of 36 and 12 km were set (denoted as d01 and d02 hereafter), and results in the finer d02 were used in the calculations of O_3 budgets. October 2015 (October 11–November 10, 2015) and July 2016 (July 1–31, 2016) were selected as the representative months in autumn and summer, respectively, for the PRD. Here, O_3 polluted days are defined when the maximum hourly O_3 concentrations exceed 200 μg/m^3, or the maximum 8-hour average O_3 concentrations exceed 160 μg/m^3 (both are the Grade-II O_3 thresholds in the Chinese National Ambient Air Quality Standard) in any municipality of the PRD. According to this definition, there were 16 and 12 O_3 polluted days in the two months, respectively (more information is given in Table S1). Further discussions focus on O_3 budgets during these days. The detailed setup of WRF-CMAQ, the validation of modelled meteorological parameters, O_3, NO_2 concentrations and hydrocarbons mixing ratios have been introduced by Qu et al. (2021). In this study, we also compared modelled ABL height, the vertical profiles of wind speed, direction and O_3 mixing ratio in Hong Kong (located in the south PRD) with corresponding observations from the IAGOS (In-service Aircraft for a Global Observing System; Petzold et al., 2015) dataset. As presented in Text S3, the acceptable modelling performance of these parameters indicates that the model provides reasonable initial data for the O_3 budget calculations.

If the calculation methods and assumptions were reasonable, the budget closure, or

$$\frac{\partial\langle c_{O_3}\rangle (or\ m_{O_3})}{\partial t} - \left(S_{htrans} + S_{ABLex} + S_{chem} + S_{cloud} + S_{ddep}\right) = 0 \quad (10)$$

would be achieved (S_{htrans}, S_{ABLex}, S_{chem}, S_{cloud} and S_{ddep} indicate the contributions of horizontal transport, vertical exchange near the ABL top, gas-phase chemistry, cloud process and dry deposition, respectively, in O_3 budgets). Therefore, we used Eq. (10) to examine the validity of the calculations. Total O_3 masses at the start and end of each hour were directly used to calculate the hourly variations of O_3 mass ($\frac{\partial m_{O_3}}{\partial t}$). Besides these, volumes at these two moments (calculated using ABL heights in all the PRD grids) were also needed to calculate the hourly variations of O_3 concentration ($\frac{\partial\langle c_{O_3}\rangle}{\partial t}$). The

contributions of various processes in the O_3 concentration and mass budgets were provided by the post-processing tool. As displayed in Fig. 2, hourly variations of O_3 concentration/mass and the corresponding net contributions from all processes show good correlations ($R^2 > 0.9$), with all fitted lines being close to the 1:1 line. Thus, the closure is met for the two O_3 budgets in both months, allowing for further analyses based on the quantified budgets.

2.6 Identifying regional sources of O_3 mass changes contributed by various processes

It is generally believed that transport (gas-phase chemistry) is closely linked to the contributions of non-local (local) emissions for O_3, but quantitative evaluation of the connections between O_3 processes and sources is still understudied. By combining O_3 budget calculations with the source apportionment method, the Brute Force Method (BFM; Clappier et al., 2017), we identified the regional sources of O_3 mass changes contributed by transport and gas-phase chemistry. Of interest were the contributions of emissions in the PRD, other regions within d02 (mainly East and Central China, short for EC-China), and regions outside d02 (the boundary conditions (BCON) of d02 modelling). The distributions of these regions are shown in Fig. S2. Besides the base scenario, three sensitivity scenarios were simulated:

- The PRD_zero scenario: Emissions in the PRD were zeroed out;
- The EC-China_zero scenario: Emissions in the EC-China were zeroed out;
- The All_zero scenario: All emissions within d02 were shut down.

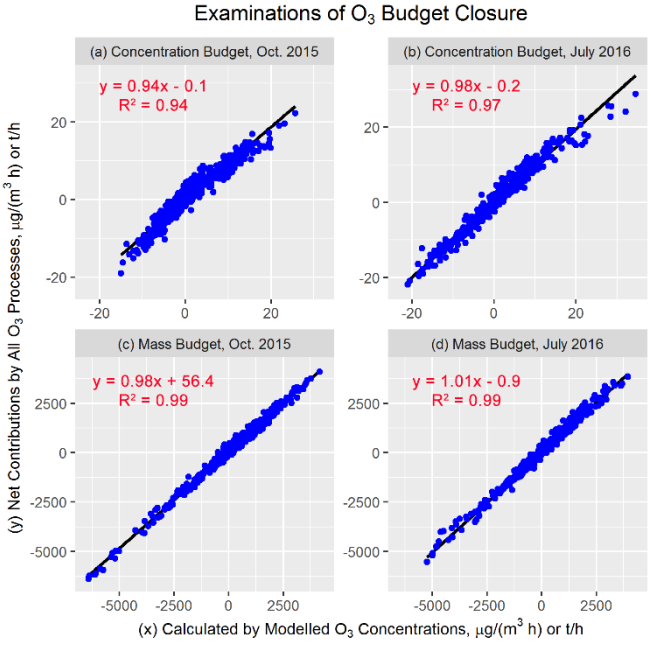

Figure 2. The examinations of O_3 budget closure in Oct. 2015 (a,c) and July 2016 (b,d) for the hourly O_3 concentration budget (a-b) and mass budget (c-d). The units for the O_3 concentration and mass budgets are µg/(m^3 h) and t/h, respectively. The solid black lines in the plots are the fitted lines.

For the process i, its hourly contributions in the O_3 mass budget in the base scenario and three sensitivity scenarios were quantified using the same method introduced in Sect. 2.2, which are marked as $f_{i,base}$, f_{i,PRD_zero}, $f_{i,EC-China\_zero}$, and f_{i,all_zero}, respectively. Then, the contributions of PRD, EC-China and BCON in O_3 mass changes attributed to the process i (separately denoted as $F_{i,PRD}$, $F_{i,EC-China}$, and $F_{i,BCON}$) were calculated as follows:

$$F_{i,PRD} = \frac{1}{2}[(f_{i,base} - f_{i,PRD\_zero}) + (f_{i,EC-China\_zero} - f_{i,all\_zero})] \quad (11)$$

$$F_{i,EC-China} = \frac{1}{2}[(f_{i,base} - f_{i,EC-China\_zero}) + (f_{i,PRD\_zero} - f_{i,all\_zero})] \quad (12)$$

$$F_{i,BCON} = f_{i,all\_zero} \quad (13)$$

In Eqs. (11) and (12), the contributions of emissions are calculated as the average results of these using top-down BFM ($(f_{i,base} - f_{i,PRD\_zero})$, $(f_{i,base} - f_{i,EC-China\_zero})$) for the PRD and EC-China emissions, respectively) and bottom-up BFM ($(f_{i,EC-China\_zero} - f_{i,all\_zero})$, $(f_{i,PRD\_zero} - f_{i,all\_zero})$) for the PRD and EC-China emissions, respectively). By doing so, the non-additivity (the sum of all contributions is not equal to the concerned metric) caused by the non-linearity between O_3 and precursors can be avoided (Qu et al., 2021).

3 Results

3.1 O_3 concentration budget

The upper panels of Fig. 3 show the diurnal changes of the O_3 concentration budget within the ABL of the PRD. According to the net contributions, O_3 concentration increased during most hours in the daytime, and its reduction at night was also considerable. We also compared the diurnal changes of ABL-mean O_3 concentration with those of observed and modelled mean near-ground O_3 concentrations in 18 sites of the Guangdong-Hong Kong-Macao PRD Regional Air Quality Monitoring Network (distributions are shown in Fig. S3). As presented in Fig. S4, three types of O_3 diurnal changes display similar characteristics. However, the budget of ABL-mean O_3 concentration can better reveal the influences of transport and photochemistry on the overall O_3 levels as well as the general causes of O_3 pollution in the targeted region. Such results in the PRD are discussed in the following.

Apparently, gas-phase chemistry controlled almost exclusively the O_3 concentration budget. During the morning hours, which are defined as the period from sunrise (~6:00 local time (LT) in autumn, ~5:00 LT in summer) to the O_3-peak hour (~14:00 LT), it (photochemistry) contributed to, on average, 74% and 95% of the O_3 concentration increase in autumn and summer, respectively. These contributions are notably higher than transport contributions (25% in autumn, 5% in summer). Gas-phase chemistry also led to the decrease of O_3 concentration at night, suggesting the impact of O_3 titration by emitted NO. It does not mean that the influence of transport on O_3 concentration can be neglected every hour. Considerable contributions of transport (mainly by ABLex-H) to O_3 increase are found 2-3 hours after sunrise, with the highest hourly

mean contributions reaching ~40% and ~25% in autumn and summer, respectively. It indicates the notable influences of air masses containing high-level O_3 entrained from residual layers. ABLex-M and horizontal transport may contribute to the increase or decrease of ABL-mean O_3 concentration, depending on the O_3 levels in air parcels transported into and out of the region (more analyses are given in Sect. 3.4). But overall, these two processes had only limited contributions to the variations of O_3 concentration. Dry deposition contributed to a considerable decrease in O_3 concentration, especially in the daytime, and served as the major sink process for O_3. To summarize, the results of the O_3 concentration budget indicate that gas-phase chemistry played a major role in the variations of O_3 concentrations in the PRD. In particular, photochemistry led to the rapid formation of O_3 pollution in the daytime, rather than transport. Our conclusions agree well with those in previous publications on the O_3 concentration budget (Lenschow et al., 1981; Hou et al., 2014; Trousdell et al., 2016; Su et al., 2018; Tan et al., 2018; Tan et al., 2019; Trousdell et al., 2019; Yu et al., 2020; Li et al., 2021a; Yan et al., 2021).

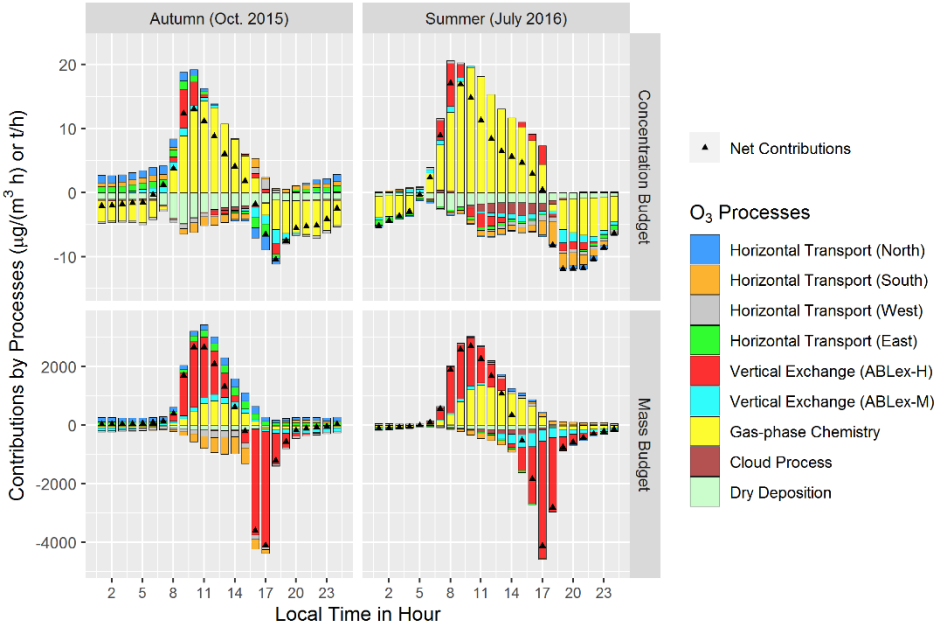

Figure 3. Mean diurnal changes of the O_3 concentration budget (the upper panels) and mass budget (the lower panels) on the polluted days of representative months in autumn (Oct. 2015; left panels) and summer (July 2016; right panels) within the atmospheric boundary layer of the Pearl River Delta. The units for the O_3 concentration and mass budgets are µg/(m^3 h) and t/h, respectively.

3.2 O_3 mass budget

The total O_3 mass within the ABL of the PRD increased during the morning hours, then decreased rapidly in the afternoon and remained stable at night in both autumn and summer (Fig. 3, the lower panels). The change of total O_3 mass agrees well with the ABL diurnal cycle (Lee, 2018) — daytime ABL development (collapse) and notable O_3 mass increase (decrease) almost occurred simultaneously, and the negligible changes in O_3 mass at night may be linked to the small variations of stable ABL.

The contribution of processes in the O_3 mass budget highlights the prominent role of transport. On average, it contributed to 78% and 53% of O_3 mass increase during the morning hours in autumn and summer, respectively, and over 90% of O_3 mass decrease during the afternoon hours of both seasons (defined as 14:00-19:00 LT in autumn and 14:00-20:00 LT in summer). Most O_3 was transported into or out of the PRD through the vertical exchange near the ABL top, especially ABLex-H, which explains the consistency between the changes of O_3 mass and ABL. The influences of ABLex-M and horizontal transport on O_3 mass were relatively limited. However, they indicated well the characteristics and variations of regional wind fields (more details are given in the next section). Gas-phase chemistry (photochemistry) also contributed to the increasing O_3 mass during the daytime, especially in summer. However, its mean contributions during the morning hours (22% in autumn, 47% in summer) were lower than those of transport. In addition, cloud process and dry deposition acted as O_3 sinks with negligible contributions to O_3 mass. Based on the above discussions, transport tends to be more important than photochemistry in the O_3 mass budget, which differs from the conclusions of the O_3 concentration budget.

The O_3 mass budget in this study overall agrees well with our common understanding of O_3 processes. The main role of transport (the vertical exchange near the ABL top) in the O_3 mass budget reflects the influence of the ABL diurnal cycle on regional O_3 pollution. Specifically, despite of relatively lower influence on O_3 concentration increase in comparison to that of photochemistry, massive O_3 being transported into the ABL during the morning hours nearly determines the regional sources of O_3 pollution. Quantified results combining O_3 mass budget and source apportionment are further discussed in Sect. 3.4.

3.3 Influences of regional wind fields on transport contributions in O_3 budgets

Through the contributions of horizontal transport and ABLex-M in O_3 budgets, the characteristics and variations of regional wind fields, including the prevailing winds and local circulations (sea breezes), can also be identified. Two main findings in this study are presented as follows:

(1) The contributions of horizontal transport and ABLex-M in autumn suggest the characteristics of prevailing winds in the PRD.

Northerly and easterly winds prevail in autumn (as indicated by the wind roses in Fig. S5). Thus, correspondingly, O_3 was transported into the PRD through its north and east borders, out of the PRD through the south and west borders, as shown in the O_3 mass budget (Fig. 3). O_3 masses transported out of the region were generally higher than those transported into the region in the daytime, which is attributed to higher downwind O_3 levels due to O_3 production from local emissions. "Low O_3 in, high O_3 out" also explains why horizontal transport led to the net decrease of O_3 concentration in the daytime. At night, O_3 was still transported into the region through the north and east borders of the PRD, but these processes became important

O_3 sources based on the O_3 concentration budget. This is to say, with relatively high O_3 levels compared to the NO_x-titrated urban atmosphere, air parcels transported from the upwind outskirts helped maintain night-time O_3 levels in the PRD to some extent.

The daytime contributions of ABLex-M in the O_3 mass budget also indicate the effects of prevailing northerly winds. The PRD has mountainous regions in the northern, western and eastern outskirts, as well as urban regions with lower altitudes in the central plain. Thus, the positive contributions of ABLex-M through the ABL top (in the z-direction) can be found in mountainous regions (Fig. S6a-b), suggesting north winds resulted in the downward transport of O_3 along the terrain. Daytime ABL heights in urban regions were, in general, higher than those in mountainous regions, which is the other reason why O_3 can be transported through the ABL slope (in the x-/y-direction) near the urban-rural interfaces when north wind prevailed (Fig. S6c-d). For the O_3 concentration budget, ABLex-M contributed to the increase of O_3 concentration during several hours after sunrise but the decrease of O_3 concentration in the afternoon. This different effect is attributed to different comparison results between ABL and above-ABL mean O_3 concentrations in the two periods (ABL < above-ABL in the morning, ABL > above-ABL in the afternoon; Fig. S7).

(2) The contributions of horizontal transport and ABLex-M in summer indicate the influence of sea breezes in the PRD.

Although southerly winds normally prevail in summer in the PRD (Fig. S5), on O_3 polluted days, air parcels from other directions could potentially influence the region as well (Qu et al., 2021). Thus the mean contribution of horizontal transport to O_3 mass in summer was lower than those in autumn. What interests us more is the different contributions of horizontal transport through the south border before and after ~14:00 LT, as indicated by the results of the O_3 mass budget. Two O_3 budgets also suggest high O_3 mass and concentration decreases contributed by ABLex-M in the afternoon. These phenomena are both related to the influence of sea breezes.

Figure 4 shows the near-ground wind roses at 14:00, 16:00 and 18:00 LT of O_3 polluted days in July 2016 based on the observational and modelling results in national meteorological sites within the PRD. At 14:00 LT, the main wind directions were W, SW and NW in both datasets. More S and SE winds occurred in later hours, and they became the prevailing winds at 18:00 LT — suggesting the gradual development of sea breezes in the PRD. Thus, O_3 was originally transported out of the PRD through the south border with negative contributions to O_3 mass; in the late afternoon, sea breezes reversed the directions of O_3 transport, resulting in positive contributions to O_3 mass by horizontal transport through the south border (Fig. 3). Moreover, sea breezes are connected to the changes of not only horizontal wind fields, but also vertical wind fields. Take the O_3 polluted day July 24th, 2016 for example, and the cross-section of O_3 concentrations and wind fields in the PRD at 16:00 LT is shown in Fig. 5 (the cross-section is made along the 113.2° E longitude, ranging from 26.0 to 20.0° N in latitude). Strong southerly wind and lower O_3 concentrations are found in the southern PRD, indicating the influence of sea

breezes on the region during that time. Near the interfaces where sea breezes encountered local air parcels (indicated by the drastic increase in O_3 levels from less than 100 μg/m^3 to about 100-150 μg/m^3), updrafts occurred, suggesting the formation of sea breeze front (Ding et al., 2004; You and Fung, 2019). It promoted the upward transport of O_3 from the ABL, or considerable O_3 mass decrease attributed to ABLex-M. The above influences of sea breezes can also be found in autumn but were weaker and occurred later.

Through the calculations and analyses of O_3 budgets, the contributions of complex transport processes in multiple scales to O_3 concentration and mass were quantified. These results can help us gain a deeper understanding of how transport influences regional O_3 pollution in the PRD.

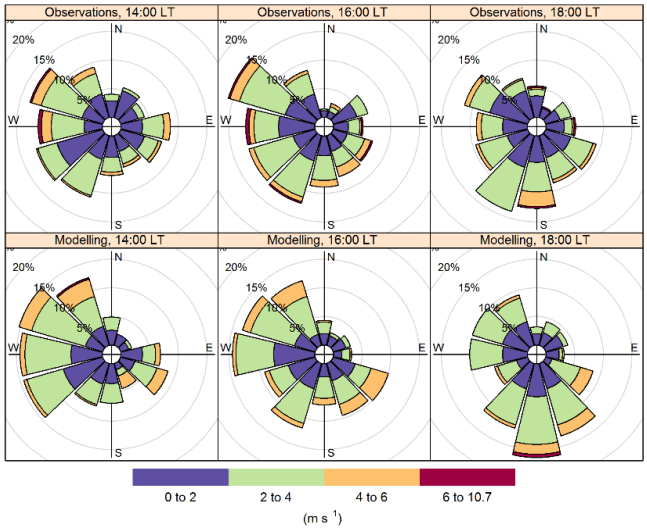

Figure 4. Wind roses at 14:00, 16:00, and 18:00 local time (LT) of the O_3 polluted days in July 2016 in the Pearl River Delta (PRD). Observational and modelling wind speeds and directions in 29 national meteorological sites within the PRD were used for this figure.

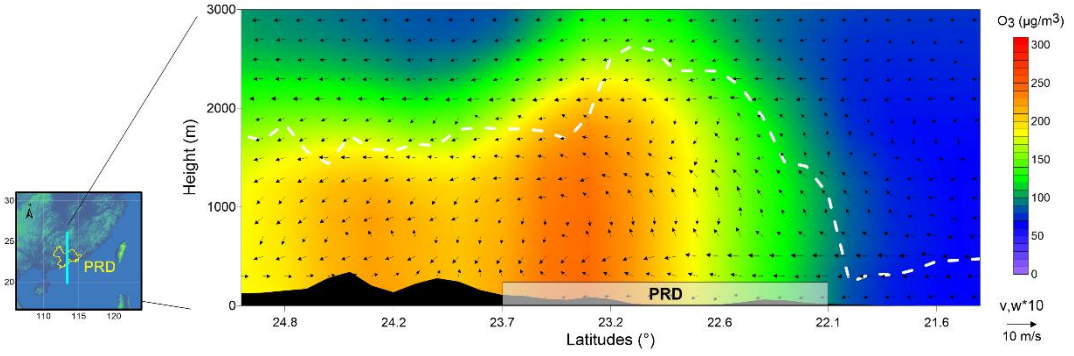

Figure 5. Cross-section of O_3 concentrations (μg/m^3) and wind fields at 16:00 local time on July 24th, 2016. The dashed white line indicates the top of the atmospheric boundary layer. PRD, Pearl River Delta.

3.4 Regional sources of O_3 mass changes contributed by transport and photochemistry

Based on previous publications (Li et al., 2012; Li et al., 2013; Yang et al., 2019; Gao et al., 2020), non-local sources often contributed to most O_3 in the PRD. This outcome is also true for the O_3 polluted days in the representative months of autumn and summer in this study, when non-local sources contributed on average to 89% and 65% of the O_3 in the PRD, respectively, in 9:00-17:00 LT (55% and 32% contributed by BCON, 34% and 33% contributed by EC-China in two months; Qu et al., 2021). To explain why non-local O_3 sources are dominant in the PRD, we identified the regional sources of O_3 mass changes contributed by the vertical exchange near the ABL top, horizontal transport and gas-phase chemistry (Fig. 6; the results in 5:00-20:00 LT are shown). Since the O_3 mass decrease overall showed similar regional sources as O_3 within the region, further analyses focus on the regional sources of O_3 mass increase, that is, O_3 transported into and produced within the PRD.

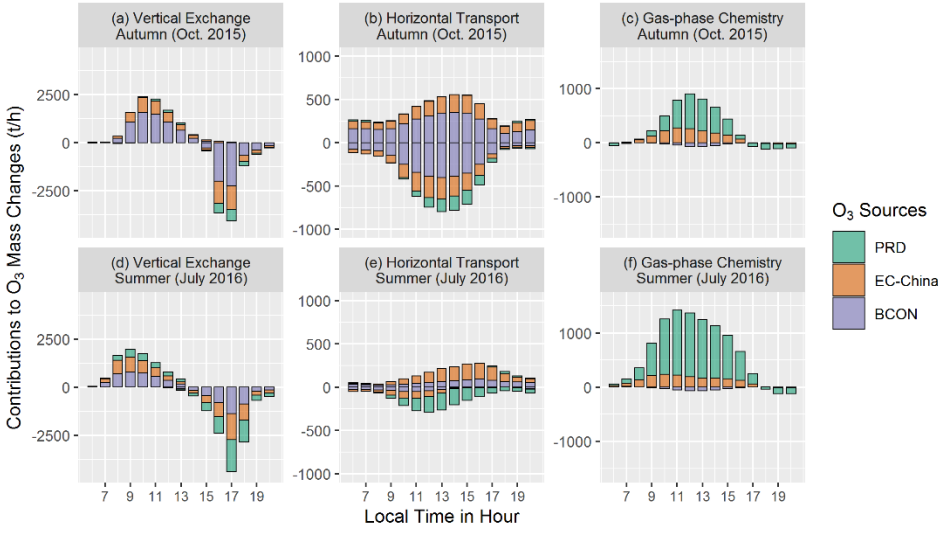

Figure 6. The regional sources of hourly O_3 mass changes contributed by (a,d) vertical exchange near the ABL top, (b,e) horizontal transport, and (c,f) gas-phase chemistry on the polluted days of representative months in autumn (Oct. 2015; a-c) and summer (July 2016; d-f). The results within 5:00-20:00 LT are shown here. PRD, Pearl River Delta; EC-China, East and Central China; BCON, the boundary conditions of d02 modelling, or the contribution of sources outside d02.

Through the vertical exchange near the ABL top, the process with the most notable contributions in the O_3 mass budget, massive non-local O_3 entered into the ABL of the PRD. In the morning-hour O_3 mass increase attributed to the process, BCON and EC-China accounted for 65% and 31%, respectively, in autumn. By contrast, local emissions only contributed to 4% in this transported O_3 during the same period, suggesting that local O_3 recirculation had only a limited influence on O_3 pollution. The results in summer were similar to those in autumn, except that the contributions of PRD (local) and EC-China emissions were higher in O_3 transported into the region through vertical exchange. In particular, local contribution accounted

for 20% in the transported O_3 during the morning hours, but was still lower than non-local contribution (38% and 42% for EC-China and BCON, respectively).

O_3 mass increase attributed to horizontal transport was connected to the contribution of non-local sources as well. In both seasons, O_3 transported into the PRD originated almost all from non-local sources.

It is not surprising that most O_3 produced through gas-phase chemistry (photochemistry) was related to local contributions, accounting for 66% and 82% during the daytime of autumn (6:00-19:00 LT) and summer (5:00-20:00 LT), respectively. However, the contributions of EC-China emissions in daytime O_3 mass increase reached 34% and 18% in two seasons, respectively, indicating the considerable influence of precursor transport on local O_3 photochemistry.

How do transport and photochemistry determine regional O_3 sources in the PRD? Based on the above results, the accumulated morning-hour O_3 mass increase exceeded 10000 t in the PRD for both seasons, which is 6-9 times larger than the original O_3 mass before sunrise (< 1500 t). Thus, daytime O_3 sources within the region were nearly determined by the sources of these newly transported and produced O_3. High contributions of transport, especially the vertical exchange near the ABL top, in O_3 mass changes as well as the dominance of non-local sources in this part of new O_3 ensured that non-local sources contributed to most O_3 in the PRD. Moreover, lower non-local contributions to O_3 in summer than in autumn can be attributed to the combined effects of higher photochemistry contributions in O_3 mass increase, lower non-local contributions in produced O_3 and higher local contributions in transported O_3. Although transport brings massive new O_3 — mostly non-local — into the region in the morning hours, it hardly leads to a drastic increase in O_3 concentration. Thus, transport seems to be less important than photochemistry in the O_3 concentration budget. Therefore, the difference between two O_3 budgets, or the different effects of transport on O_3 concentration and mass, may result in distinct understandings about the role of transport and photochemistry in regional O_3 pollution.

4 Conclusion and outlook

Reported O_3 budgets and source apportionments often concluded with a conflicting role of transport and photochemistry in ambient O_3 pollution. To explore its causes, we used the modelling results of WRF-CMAQ to quantify the contributions of various processes in the O_3 concentration and mass budgets. Results in the PRD revealed that gas-phase chemistry, including daytime photochemistry and night-time O_3 titration, drives the variations of O_3 concentration. Particularly, the former separately contributed to 74% and 95% of O_3 concentration increase in the morning of autumn and summer months. In contrast, transport, especially the vertical exchange near the ABL top, is the main process contributing to the O_3 mass increase in the morning (78% and 53% in autumn and summer, respectively) and its decrease in the afternoon (> 90%). The diurnal changes of transport contributions in two O_3 budgets are closely connected to the variations of ABL and regional

wind fields, including the prevailing winds and local circulations (sea breezes), in the PRD. Although massive O_3 transported into the ABL in the morning has a relatively limited influence on O_3 concentration increase (25% and 5% in autumn and summer, respectively) compared to photochemistry, it nearly determines the dominance of non-local sources for daytime O_3 in the PRD. The difference between two O_3 budgets, or the different effects of transport on O_3 concentration and mass, may explain why the roles of transport and photochemistry in regional O_3 pollution are inconsistent between different studies.

It should be noted that the conclusions in this study apply not only to tropospheric O_3 but also to other pollutants with moderately long atmospheric lifetimes, such as some of the secondary components in fine particulate matter. Transport and chemical transformation are both important processes for these pollutants, but for the former, it has different influences on the concentration and mass of pollutants on an hourly scale. Besides regional sources, in theory, the difference between the two budgets may also contribute to the inconsistency of other pollutant characteristics identified using different methods, such as the reaction pathways and sensitivities to precursor emissions. When pollutants with different characteristics are massively transported into the region, the variation of their concentrations is often not notable and thus neglected in the concentration budgets. However, according to the discussions in this study, the transport process is likely to change or even determine the characteristics of pollutants within the region. It also makes the considerable impacts of relatively slow chemistry along the transport on local pollution possible. Therefore, we suggested that attention should be paid to selecting a proper budget type and using correct budget calculation methods in related research.

Uncertainty remains in the calculated O_3 budgets, which is partly related to the biases in the modelling results. Therefore, supporting observations are essential for future research. Recent progress in observational techniques (Zhao et al., 2021; Zhou et al., 2021) has enabled three-dimensional measurements of meteorological parameters and O_3 concentrations with high spatiotemporal resolution and coverage. These data can be used not only in the model validation of key parameters in budget calculations, but also in the comparisons between observation- and modelling-based contributions by various processes in O_3 budgets. By doing so, more accurate regional-level O_3 budgets will be obtained.

This study concluded that transport and gas-phase chemistry play the main role in the O_3 concentration and mass budgets, respectively. Based on the two O_3 budgets, we suggest that emission reduction in the upwind regions can effectively lower daily-mean O_3 levels due to its high contributions to regional O_3, but a longer time is needed due to the slow response of O_3 concentration to transport. By contrast, reducing local emissions hinders rapid daytime O_3 concentration increase and lowers O_3 peak levels efficiently in the short term. The choice of which strategy to apply should depend on the specific goals of O_3 control (mean levels vs. peak levels; long-term vs. short-term), which are set based on a more in-depth understanding of O_3 effects on human health, crop yields and ecosystems. More efforts are required to systematically evaluate the effects of different emission reduction strategies on alleviating the detrimental effects of ambient O_3.

Data availability. The source codes of WRF and CMAQ are available at the site https://www2.mmm.ucar.edu/wrf/users/download/get_sources.html and https://www.cmascenter.org/cmaq/, respectively. FNL meteorological input files were downloaded from the site https://rda.ucar.edu/datasets/ds083.2/. MEIC v1.3 anthropogenic emission inventory is available at http://meicmodel.org/?page_id=560. The source codes of MEGAN can be found at https://bai.ess.uci.edu/megan/data-and-code. IAGOS dataset used in model validation was searched and downloaded from http://iagos-data.fr, which includes all profiles measured in flights taking off from and landing in Hong Kong during two representative months. We also provided the initial Fortran code used in ozone budget calculations and hourly O_3 concentration and mass budget results in two representative months (the initial data of Fig. 3) at https://doi.org/10.5281/zenodo.6259253.

Author contributions. KQ, XW and YZ designed the study. KQ, XW, TX did the simulations using the WRF-CMAQ model. JS, LZ and YZ provided observational results for model validation. KQ, XW, XC, YY, XJ and YZ developed the post-processing tool, conducted and analysed O_3 budget results. KQ, XW, MV and YZ wrote and revised this paper, with critical feedbacks from all other authors.

Competing interests. The authors declare no conflict of interest.

Acknowledgements. This study was supported by the National Key Research and Development Program of China (grant No. 2018YFC0213204), the National Science and Technology Pillar Program of China (grant No. 2014BAC21B01) and the co-funded DFG-NSFC Sino-German AirChanges project (grant No. 448720203).

References

Ainsworth, E. A.: Understanding and improving global crop response to ozone pollution, Plant J., 90, 886–897, https://doi.org/10.1111/tpj.13298, 2017.

Bates, K. H. and Jacob, D. J.: An expanded definition of the odd oxygen family for tropospheric ozone budgets: Implications for ozone lifetime and stratospheric influence, Geophys. Res. Lett., 47, e2019GL084486, https://doi.org/10.1029/2019GL084486, 2019.

Boian, C. and Andrade, M. D. F.: Characterization of ozone transport among metropolitan regions, Rev. Bras. Meteorol., 27, 229-242, https://doi.org/10.1590/S0102-77862012000200009, 2012.

Chang, X., Wang, S., Zhao, B., Cai, S., and Hao, J.: Assessment of inter-city transport of particulate matter in the Beijing–Tianjin–Hebei region, Atmos. Chem. Phys., 18, 4843–4858, https://doi.org/10.5194/acp-18-4843-2018, 2018.

Clappier, A., Belis, C. A., Pernigotti, D., and Thunis, P.: Source apportionment and sensitivity analysis: two methodologies with two different purposes, Geosci. Model Dev., 10, 4245–4256, https://doi.org/10.5194/gmd-10-4245-2017, 2017.

Ding, A., Wang, T., Zhao, M., Wang, T. J., and Li, Z. K.: Simulation of sea-land breezes and a discussion of their implications on the transport of air pollution during a multi-day ozone episode in the Pearl River Delta of China, Atmos. Environ., 38, 6737–6750, https://doi.org/10.1016/j.atmosenv.2004.09.017, 2004.

Fishman, J., Wozniak, A. E., and Creilson, J. K.: Global distribution of tropospheric ozone from satellite measurements using the empirically corrected tropospheric ozone residual technique: Identification of the regional aspects of air pollution, Atmos. Chem. Phys., 3, 893–907, https://doi.org/10.5194/acp-3-893-2003, 2003.

Fleming, Z. L., Doherty, R. M., von Schneidemesser, E., Malley, C. S., Cooper, O. R., Pinto, J. P., Colette, A., Xu, X. B., Simpson, D., Schultz, M. G., Lefohn, A. S., Hamad, S., Moolla, R., Solberg, S., and Feng, Z. Z.: Tropospheric ozone assessment report: Present-day ozone distribution and trends relevant to human health, Elementa-Sci. Anthrop., 6, 12, https://doi.org/10.1525/elementa.273, 2018.

Fowler, D., Brimblecombe, P., Burrows, J., Heal, M. R., Grennfelt, P., Stevenson, D. S., Jowett, A., Nemitz, E., Coyle, M., Liu, X., Chang, Y., Fuller, G. W., Sutton, M. A., Klimont, Z., Unsworth, M. H., and Vieno, M.: A chronology of global air quality, Philos. T. R. Soc. A, 378, 20190314, https://doi.org/10.1098/rsta.2019.0314, 2020.

Gao, M., Gao, J., Zhu, B., Kumar, R., Lu, X., Song, S., Zhang, Y., Jia, B., Wang, P., Beig, G., Hu, J., Ying, Q., Zhang, H., Sherman, P., and McElroy, M. B.: Ozone pollution over China and India: seasonality and sources, Atmos. Chem. Phys., 20, 4399–4414, https://doi.org/10.5194/acp-20-4399-2020, 2020.

Gao, X., Deng, X., Tan, H., Wang, C., Wang, N., and Yue, D.: Characteristics and analysis on regional pollution process and circulation weather types over Guangdong Province, Acta Scientiae Circumstantiae (in Chinese), 38(5), 1708–1716, https://doi.org/10.13671/j.hjkxxb.2017.0473, 2018.

Guo, J. J., Fiore, A. M., Murray, L. T., Jaffe, D. A., Schnell, J. L., Moore, C. T., and Milly, G. P.: Average versus high surface ozone levels over the continental USA: model bias, background influences, and interannual variability, Atmos. Chem. Phys., 18, 12123–12140, https://doi.org/10.5194/acp-18-12123-2018, 2018.

Hou, X., Zhu, B., Kang, H., and Gao, J.: Analysis of seasonal ozone budget and spring ozone latitudinal gradient variation in the boundary layer of the Asia-Pacific region, Atmos. Environ., 94, 734–741, https://doi.org/10.1016/j.atmosenv.2014.06.006, 2014.

Hu, J., Li, Y., Zhao, T., Liu, J., Hu, X.-M., Liu, D., Jiang, Y., Xu, J., and Chang, L.: An important mechanism of regional O_3 transport for summer smog over the Yangtze River Delta in eastern China, Atmos. Chem. Phys., 18, 16239–16251, https://doi.org/10.5194/acp-18-16239-2018, 2018.

Janssen, R. H. H. and Pozzer, A.: Description and implementation of a MiXed Layer model (MXL, v1.0) for the dynamics of the atmospheric boundary layer in the Modular Earth Submodel System (MESSy), Geosci. Model Dev., 8, 453–471, https://doi.org/10.5194/gmd-8-453-2015, 2015.

Jin, X., Cai, X., Huang, Q., Wang, X., Song, Y., and Zhu, T.: Atmospheric boundary layer—free troposphere air exchange in the North China Plain and its impact on $PM_{2.5}$ pollution, J. Geophys. Res.-Atmos., 126(9), e2021JD034641, https://doi.org/10.1029/2021JD034641, 2021.

Kaser, L., Patton, E. G., Pfister, G. G., Weinheimer, A. J., Montzka, D. D., Flocke, F., Thompson, A. M., Stauffer, R. M., and Halliday, H. S.: The effect of entrainment through atmospheric boundary layer growth on observed and modeled surface ozone in the Colorado Front Range, J. Geophys. Res.-Atmos., 122, 6075–6093, https://doi.org/10.1002/2016JD026245, 2017.

Kulmala, M., Kokkonen, T. V., Pekkanen, J., Paatero, S., Petäjä, T., Kerminen, V.-M., and Ding, A.: Opinion: Gigacity – a source of problems or the new way to sustainable development, Atmos. Chem. Phys., 21, 8313–8322, https://doi.org/10.5194/acp-21-8313-2021, 2021.

Lee, X.: Fundamentals of Boundary-Layer Meteorology, Springer Atmospheric Sciences., 2018.

Lelieveld, J., Hoor, P., Jöckel, P., Pozzer, A., Hadjinicolaou, P., Cammas, J.-P., and Beirle, S.: Severe ozone air pollution in the Persian Gulf region, Atmos. Chem. Phys., 9, 1393–1406, https://doi.org/10.5194/acp-9-1393-2009, 2009.

Lenschow, D. H., Pearson, R., and Stankov, B. B.: Estimating the ozone budget in the boundary layer by use of aircraft measurements of ozone eddy flux and mean concentration, J. Geophys. Res., 86, 7291–7297, https://doi.org/10.1029/JC086iC08p07291, 1981.

Li, A., Zhou, Q., and Xu, Q.: Prospects for ozone pollution control in China: An epidemiological perspective, Environ. Pollut., 285, 117670, https://doi.org/10.1016/j.envpol.2021.117670, 2021b.

Li, L., Xie, F., Li, J., Gong, K., Xie, X., Qin, Y., Qin, M., and Hu, J.: Diagnostic analysis of regional ozone pollution in Yangtze River Delta, China: A case study in summer 2020, Sci. Total Environ., 812, 151511, https://doi.org/10.1016/j.scitotenv.2021.151511, 2021a.

Li, Y., Lau, A. K. H., Fung, J. C. H., Ma, H., and Tse, Y.: Systematic evaluation of ozone control policies using an Ozone Source Apportionment method, Atmos. Environ., 76, 136–146, https://doi.org/10.1016/j.atmosenv.2013.02.033, 2013.

Li, Y., Lau, A. K. H., Fung, J. C. H., Zheng, J.Y., Zhong, L. J., and Louie, P. K. K.: Ozone source apportionment (OSAT) to differentiate local regional and super-regional source contributions in the Pearl River Delta region, China, J. Geophys. Res.-Atmos., 117, D15305, http://doi.org/10.1029/2011JD017340, 2012.

Liu, H. L., Zhang, M. G., and Han, X.: A review of surface ozone source apportionment in China, Atmos. Ocean. Sci. Lett., 13, 470–484, https://doi.org/10.1080/16742834.2020.1768025, 2020.

Liu, P., Zhang, Y., Yu, S. C., and Schere, K. L.: Use of a Process Analysis tool for diagnostic study on fine particulate matter predictions in the U.S. Part II: Process Analysis and sensitivity simulations, Atmos. Pollut. Res., 2, 61–71, https://doi.org/10.5094/APR.2011.008, 2011.

Lu, X., Hong, J., Zhang, L., Cooper, O. R., Schultz, M. G., Xu, X., Wang, T., Gao, M., Zhao, Y., and Zhang, Y.: Severe surface ozone pollution in China: A global perspective, Environ. Sci. Tech. Let., 5(8), 487–494, https://doi.org/10.1021/acs.estlett.8b00366, 2018.

Massagué, J., Carnerero, C., Escudero, M., Baldasano, J. M., Alastuey, A., and Querol, X.: 2005–2017 ozone trends and potential benefits of local measures as deduced from air quality measurements in the north of the Barcelona metropolitan area, Atmos. Chem. Phys., 19, 7445–7465, https://doi.org/10.5194/acp-19-7445-2019, 2019.

Mills, G., Wagg, S., and Harmens, H.: Ozone pollution: impacts on ecosystem services and biodiversity (CEH Project no. C04062, C04325), Bangor, UK, NERC/Centre for Ecology & Hydrology, 2013.

Naik, V., Szopa, S., Adhikary, B., Artaxo, P., Berntsen, T., Collins, W. D., Fuzzi, S., Gallardo, L., Kiendler Scharr, A., Klimont, Z., Liao, H., Unger, N., and Zanis, P.: Short-Lived Climate Forcers, in: Climate Change 2021: The Physical Science Basis. Contribution of Working Group I to the Sixth Assessment Report of the Intergovernmental Panel on Climate Change, edited by: Masson-Delmotte, V., Zhai, P., Pirani, A., Connors, S. L., Péan, C., Berger, S., Caud, N., Chen, Y., Goldfarb, L., Gomis, M. I., Huang, M., Leitzell, K., Lonnoy, E., Matthews, J. B. R., Maycock, T. K., Waterfield, T., Yelekçi, O., Yu, R., and Zhou, B., Cambridge University Press, Cambridge, United Kingdom and New York, NY, USA, 817–922, https://doi.org/10.1017/9781009157896.008, 2021.

Novel, D. P.: The OTC challenge: Adding VOC controls in the northeast, J. Air Waste Manag. Assoc., 42(8), 1053-1056, https://doi.org/10.1080/10473289.1992.10467050, 1992.

Pay, M. T., Gangoiti, G., Guevara, M., Napelenok, S., Querol, X., Jorba, O., and Pérez García-Pando, C.: Ozone source apportionment during peak summer events over southwestern Europe, Atmos. Chem. Phys., 19, 5467–5494, https://doi.org/10.5194/acp-19-5467-2019, 2019.

Petzold, A., Thouret, V., Gerbig, C., Zahn, A., Brenninkmeijer, C. A. M., Gallagher, M., Hermann, M., Pontaud, M., Ziereis, H., Boulanger, D., Marshall, J., Nédélec, P., Smit, H. G. J., Friess, U., Flaud, J.-M., Wahner, A., Cammas, J.-P., Volz-Thomas, A. and IAGOS TEAM: Global-scale atmosphere monitoring by in-service aircraft–current achievements and

future prospects of the European Research Infrastructure IAGOS, Tellus B, 67, 28452, https://doi.org/10.3402/tellusb.v67.28452, 2015.

Qu, K., Wang, X., Yan, Y., Shen, J., Xiao, T., Dong, H., Zeng, L., and Zhang, Y.: A comparative study to reveal the influence of typhoons on the transport, production and accumulation of O_3 in the Pearl River Delta, China, Atmos. Chem. Phys., 21, 11593–11612, https://doi.org/10.5194/acp-21-11593-2021, 2021.

Reid, N., Yap, D., and Bloxam, R.: The potential role of background ozone on current and emerging air issues: An overview, Air Qual. Atmos. Health, 1, 19–29, https://doi.org/10.1007/s11869-008-0005-z, 2008.

Schultz, M. G., Schröder, S., Lyapina, O., Cooper, O., Galbally, I., Petropavlovskikh, I., Von Schneidemesser, E., Tanimoto, H., Elshorbany, Y., Naja, M., Seguel, R., Dauert, U., Eckhardt, P., Feigenspahn, S., Fiebig, M., Hjellbrekke, A.-G., Hong, Y.-D., Kjeld, P. C., Koide, H., Lear, G., Tarasick, D., Ueno, M., Wallasch, M., Baumgardner, D., Chuang, M.-T., Gillett, R., Lee, M., Molloy, S., Moolla, R., Wang, T., Sharps, K., Adame, J. A., Ancellet, G., Apadula, F., Artaxo, P., Barlasina, M., Bogucka, M., Bonasoni, P., Chang, L., Colomb, A., Cuevas, E., Cupeiro, M., Degorska, A., Ding, A., Fröhlich, M., Frolova, M., Gadhavi, H., Gheusi, F., Gilge, S., Gonzalez, M. Y., Gros, V., Hamad, S. H., Helmig, D., Henriques, D., Hermansen, O., Holla, R., Huber, J., Im, U., Jaffe, D. A., Komala, N., Kubistin, D., Lam, K.-S., Laurila, T., Lee, H., Levy, I., Mazzoleni, C., Mazzoleni, L., McClure-Begley, A., Mohamad, M., Murovic, M., Navarro-Comas, M., Nicodim, F., Parrish, D., Read, K. A., Reid, N., Ries, L., Saxena, P., Schwab, J. J., Scorgie, Y., Senik, I., Simmonds, P., Sinha, V., Skorokhod, A., Spain, G., Spangl, W., Spoor, R., Springston, S. R., Steer, K., Steinbacher, M., Suharguniyawan, E., Torre, P., Trickl, T., Weili, L., Weller, R., Xu, X., Xue, L., and Zhiqiang, M.: Tropospheric ozone assessment report: Database and metrics data of global surface ozone observations, Elementa-Sci. Anthrop., 5, 58, https://doi.org/10.1525/elementa.244, 2017.

Sinclair, V. A., Belcher, S. E., and Gray, S. L.: Synoptic controls on boundary-layer characteristics, Bound.-Layer Meteorol., 134, 387–409, https://doi.org/10.1007/s10546-009-9455-6, 2010.

Sitch, S., Cox, P. M., Collins, W. J., and Huntingford, C.: Indirect radiative forcing of climate change through ozone effects on the land-carbon sink, Nature, 448, 791–795, https://doi.org/10.1038/nature06059, 2007.

Stevenson, D. S., Dentener, F. J., Schultz, M. G., Ellingsen, K., van Noije, T. P. C., Wild, O., Zeng, G., Amann, M., Atherton, C. S., Bell, N., Bergmann, D. J., Bey, I., Butler, T., Cofala, J., Collins, W. J., Derwent, R. G., Doherty, R. M., Drevet, J., Eskes, H. J., Fiore, A. M., Gauss, M., Hauglustaine, D. A., Horowitz, L. W., Isaksen, I. S. A., Krol, M. C., Lamarque, J.-F., Lawrence, M. G., Montanaro, V., Müller, J.-F., Pitari, G., Prather, M. J., Pyle, J. A., Rast, S., Rodriguez, J. M., Sanderson, M. G., Savage, N. H., Shindell, D. T., Strahan, S. E., Sudo, K., and Szopa, S.: Multimodel ensemble simulations of present-day and near-future tropospheric ozone, J. Geophys. Res., 111, D08301, https://doi.org/10.1029/2005JD006338, 2006.

Su, R., Lu, K. D., Yu, J. Y., Tan, Z. F., Jiang, M. Q., Li, J., Xie, S. D., Wu, Y. S., Zeng, L. M., Zhai, C. Z., and Zhang, Y. H.: Exploration of the formation mechanism and source attribution of ambient ozone in Chongqing with an observation-based model, Sci. China Earth Sci., 61, 23–32, https://doi.org/10.1007/s11430-017-9104-9, 2018.

Tan, Z., Lu, K., Jiang, M., Su, R., Dong, H., Zeng, L., Xie, S., Tan, Q., and Zhang, Y.: Exploring ozone pollution in Chengdu, southwestern China: A case study from radical chemistry to O_3-VOC-NO_x sensitivity, Sci. Total Environ., 636, 775–786, https://doi.org/10.1016/j.scitotenv.2018.04.286, 2018.

Tan, Z., Lu, K., Jiang, M., Su, R., Wang, H., Lou, S., Fu, Q., Zhai, C., Tan, Q., Yue, D., Chen, D., Wang, Z., Xie, S., Zeng, L., and Zhang, Y.: Daytime atmospheric oxidation capacity in four Chinese megacities during the photochemically polluted season: a case study based on box model simulation, Atmos. Chem. Phys., 19, 3493–3513, https://doi.org/10.5194/acp-19-3493-2019, 2019.

Tang, G., Liu, Y., Huang, X., Wang, Y., Hu, B., Zhang, Y., Song, T., Li, X., Wu, S., Li, Q., Kang, Y., Zhu, Z., Wang, M., Wang, Y., Li, T., Li, X., and Wang, Y.: Aggravated ozone pollution in the strong free convection boundary layer, Sci. Total Environ., 788, 147740, https://doi.org/10.1016/j.scitotenv.2021.147740, 2021.

Tang, G. Q., Zhu, X. W., Xin, J. Y., Hu, B., Song, T., Sun, Y., Zhang, J. Q., Wang, L. L., Cheng, M. T., Chao, N., Kong, L. B., Li, X., and Wang, Y. S.: Modelling study of boundary-layer ozone over northern China – Part I: Ozone budget in summer, Atmos. Res., 187, 128–137, https://doi.org/10.1016/j.atmosres.2016.10.017, 2017.

Thunis, P., Clappier, A., Tarrason, L., Cuvelier, C., Monteiro, A., Pisoni, E., Wesseling, J., Belis, C. A., Pirovano, G., Janssen, S., Guerreiro, C., and Peduzzi, E.: Source apportionment to support air quality planning: Strengths and weaknesses of existing approaches, Environ. Int., 130, 104825, https://doi.org/10.1016/j.envint.2019.05.019, 2019.

Trousdell, J. F., Caputi, D., Smoot, J., Conley, S. A., and Faloona, I. C.: Photochemical production of ozone and emissions of NO_x and CH_4 in the San Joaquin Valley, Atmos. Chem. Phys., 19, 10697–10716, https://doi.org/10.5194/acp-19-10697-2019, 2019.

Trousdell, J. F., Conley, S. A., Post, A., and Faloona, I. C.: Observing entrainment mixing, photochemical ozone production, and regional methane emissions by aircraft using a simple mixed-layer framework, Atmos. Chem. Phys., 16, 15433–15450, https://doi.org/10.5194/acp-16-15433-2016, 2016.

Vilà-Guerau De Arellano, J., van Heerwaarden, C. C., van Stratum, B. J. H., and van den Dries, K.: Atmospheric Boundary Layer: Integrating Air Chemistry and Land Interactions, Cambridge University Press, New York, 2015.

Yan, F., Gao, Y., Ma, M., Liu, C., Ji, X., Zhao, F., Yao, X., and Gao, H.: Revealing the modulation of boundary conditions and governing processes on ozone formation over northern China in June 2017, Environ. Pollut., 272, 115999, https://doi.org/10.1016/j.envpol.2020.115999, 2021.

Yang, L., Wang, X., and Chen, Q.: New method for investigating regional interactions of air pollutants (in Chinese), Acta Sci. Circumstantiae, 32(3), 528-536, https://doi.org/10.13671/j.hjkxxb.2012.03.012, 2012.

Yang, W., Chen, H., Wang, W., Wu, J., Li, J., Wang, Z., Zheng, J., and Chen, D.: Modeling study of ozone source apportionment over the Pearl River Delta in 2015, Environ. Pollut., 253, 393-402, https://doi.org/10.1016/j.envpol.2019.06.091, 2019.

You, C., and Fung, J. C. H.: Characteristics of the sea-breeze circulation in the Pearl River Delta region and its dynamical diagnosis. Journal of Applied Meteorology and Climatology, 58(4), 741-755, https://doi.org/10.1175/JAMC-D-18-0153.1, 2019.

Yu, D., Tan, Z., Lu, K., Ma, X., Li, X., Chen, S., Zhu, B., Lin, L., Li, Y., Qiu, P., Yang, X., Liu, Y., Wang, H., He, L., Huang, X., and Zhang, Y.: An explicit study of local ozone budget and NO_x-VOCs sensitivity in Shenzhen China, Atmos. Environ., 224, 117304, https://doi.org/10.1016/j.atmosenv.2020.117304, 2020.

Zhang, J. J., Wei, Y., and Fang, Z.: Ozone pollution: A major health hazard worldwide, Front. Immunol., 10, 2518, https://doi.org/10.3389/fimmu.2019.02518, 2019.

Zhao, R., Hu, Q., Sun, Z., Wu, Y., Xing, C., Liu, H., and Liu, C., (2021). Review of space and ground integrated remote sensing for air pollutants (in Chinese). Res. Environ. Sci., 34(1), 28-40. https://doi.org/10.13198/j.issn.1001-6929.2020.11.25, 2021.

Zhao, W., Tang, G., Yu, H., Yang, Y., Wang, Y., Wang, L., An, J., Gao, W., Hu, B., Cheng, M., An, X., Li, X., and Wang, Y.: Evolution of boundary layer ozone in Shijiazhuang, a suburban site on the North China Plain, J. Environ. Sci., 83, 152–160, https://doi.org/10.1016/j.jes.2019.02.016, 2019.

Zhou, B., Zhang, S., Xue, R., Li, J., and Wang, S.: A review of Space-Air-Ground integrated remote sensing techniques for atmospheric monitoring, J. Environ. Sci., https://doi.org/10.1016/j.jes.2021.12.008, 2021.

Supplement of

Rethinking the role of transport and photochemistry in regional ozone pollution: Insights from ozone concentration and mass budgets

Kun Qu[1,2,3], Xuesong Wang[1,2], Xuhui Cai[1,2], Yu Yan[1,2], Xipeng Jin[1,2], Mihalis Vrekoussis[3,4,5], Jin Shen[6], Teng Xiao[1,2], Limin Zeng[1,2], and Yuanhang Zhang[1,2,7,8]

[1]State Key Joint Laboratory of Environmental Simulation and Pollution Control, College of Environmental Sciences and Engineering, Peking University, Beijing 100871, China
[2]International Joint Laboratory for Regional Pollution Control, Ministry of Education, Beijing, 100816, China
[3]Laboratory for Modelling and Observation of the Earth System (LAMOS), Institute of Environmental Physics (IUP), University of Bremen, Bremen, Germany
[4]Center of Marine Environmental Sciences (MARUM), University of Bremen, Germany
[5]Climate and Atmosphere Research Center (CARE-C), The Cyprus Institute, Cyprus
[6]State Key Laboratory of Regional Air Quality Monitoring, Guangdong Key Laboratory of Secondary Air Pollution Research, Guangdong Environmental Monitoring Center, Guangzhou 510308, China
[7]Beijing Innovation Center for Engineering Science and Advanced Technology, Peking University, Beijing 100871, China
[8]CAS Center for Excellence in Regional Atmospheric Environment, Chinese Academy of Sciences, Xiamen 361021, China

Correspondence to: Xuesong Wang (xswang@pku.edu.cn) and Yuanhang Zhang (yhzhang@pku.edu.cn)

Contents

Three texts, ten figures and two tables are included in this Supporting Information for the paper entitled "Rethinking the role of transport and photochemistry in regional ozone pollution: Insights from ozone mass and concentration budgets".

For texts:

- Text S1 describes the detailed processes of O_3 budget calculations in this study.
- Text S2 compares the equations of O_3 budget calculations used in this study with these in 1-D models.
- Text S3 presents the results of model validation of atmospheric boundary layer (ABL) height, wind and O_3 mixing profiles based on the IAGOS dataset.

For figures:

- Figure S1 indicates two calculation paths for the regional O_3 concentration budget within an hour.
- Figure S2 displays the spatial distributions of the second modelling domain (d02) and source regions.
- Figure S3 presents the spatial distributions of 18 sites of the Guangdong-Hong Kong-Macao Pearl River Delta (PRD) Regional Air Quality Monitoring Network.
- Figure S4 compared the mean diurnal changes of O_3 concentrations in the PRD from three sources: observational near-ground O_3 concentrations, modelled near-ground O_3 concentrations and ABL-mean O_3 concentrations.
- Figure S5 compares IAGOS and modelling wind roses in Hong Kong in the two representative months.
- Figure S6 displays the spatial distributions of mean contributions of vertical exchange near the ABL top due to large-scale air motion (ABLex-M) to O_3 mass changes in the morning and afternoon of two representative months.
- Figure S7 compares IAGOS and CMAQ modelling vertical profiles of O_3 mixing ratios in Hong Kong in the two representative months.
- Figure S8 is the flow diagram of the O_3 budget calculation processes.
- Figure S9 is the flow diagram of the O_3 budget calculation in Step I (or the post-processing tool *flux_4d_cal*).
- Figure S10 shows the comparison results between IAGOS and modelling atmospheric boundary layer height in Hong Kong in Oct. 2015.

For tables:

- Table 1 gives more detailed information on the O_3 polluted days of the PRD in the two representative months.
- Table 2 lists the formulas in the O_3 budget calculations, the parameters used and their corresponding source files in the *flux_4d_cal* tool.

Text S1. Detailed processes of O_3 budget calculations

As the flow diagram shown in Fig. S8, there are two steps in the calculations of O_3 budgets based on the WRF-CMAQ modelling results:

1) Step I: Quantifications of transport fluxes and volume

The post-processing tool *flux_4d_cal* was developed using FORTRAN90 for this step. For all grid columns except for those next to the boundaries of the modelling domain, the calculation contents in the tool include:

- Hourly contributions of horizontal transport to O_3 mass changes within the ABL, including these in the x- and y-directions;
- Hourly contributions of vertical exchange due to the changes of ABL height (ABLex-H) to O_3 mass changes within the ABL;
- Hourly contributions of vertical exchange due to large-scale air motion (ABLex-M) to O_3 mass changes within the ABL, including these in the x-, y- and z-directions;
- Hourly contributions of other processes (gas-phase chemistry, cloud process and dry deposition) to O_3 mass changes within the ABL;
- Hourly transported air volumes by each transport process;
- Total O_3 masses within the ABL at both the start and end of each hour;
- ABL heights at the starting and end hours.

All of the above values can be found in the NetCDF (nc) output files, and they are used in the Step II calculations.
To finish the calculations of Step I, several input files are needed:

- Meteorological files processed by the MCIP module in CMAQ from the WRF outputs, which include the METCRO2D (meteorological parameters in the 2-D space), METCRO3D (meteorological parameters in the 3-D space) and MERDOT3D (wind speeds in the 3-D space) files;
- Pollutant concentration output files (CONC files) modelled by CMAQ, where hourly O_3 concentrations are stored;
- Process Analysis (PA) output files modelled by CMAQ, where the hourly, nested contributions of gas-phase chemistry, cloud process and dry deposition to O_3 concentration are stored.

For most of the files used here, the setting of spatial domains and times should be consistent; otherwise, the calculations would not be performed or generate wrong results. Additionally, users should provide the resolution of the modelling domain and the orders of contributions by three non-transport O_3 processes in the PA files for further calculations.
The flow chart of the calculation in *flux_4d_cal* is shown in Fig. S9. The calculation formulas for the grid column (*i*, *j*), parameters used and their source files are summarized in Table S2. There are four loops in the calculations, which are the

loops of x-, y-grids, time steps and vertical layers. We assume that there are 60 time-steps within an hour, and parameters at each time step can be interpolated linearly by their values at the starting and end hours. The hourly contribution of non-transport processes to O_3 in a grid cell is divided equally to these within each time step. For every layer within the ABL, fluxes and volumes related to horizontal transport and non-transport processes are calculated and summed up. For layers where the ABL top is located, besides these aforementioned parameters, contributions to O_3 mass changes and volumes related to vertical exchange (ABLex-H and ABLex-M) are also calculated. Total O_3 masses within the ABL at the start and end of each hour are directly calculated, and ABL heights at the starting and end hours can be read from the METCRO2D files.

The height of night-time stable ABL can be severely underestimated by normally used ABL parameterization, especially when the Richardson number is used (Dai et al., 2014). To reduce the influence of imprecise ABL heights in the O_3 budget calculations, here, we set the lowest ABL height limit as 350 m for all hours, which is an approximate value close to the values reported by night-time observations in summer or autumn in the Pearl River Delta (Chan et al., 2006; Fan et al., 2011; He et al., 2021; Song et al., 2021). The results of the budget closure examination (Fig. 2 in the manuscript) also suggest that the choice of this value is acceptable. Further studies are surely needed to determine this value better. However, we focus on the causes of daytime ozone pollution; thus, night-time budgets do not notably influence the conclusions of this study.

2) Step II: Regional O_3 budget calculations and closure examinations

This step aims to: 1) calculate the hourly O_3 mass and concentration budgets within the ABL of the user-defined regions and 2) check whether the closure between the changes of O_3 masses/concentrations modelled by CMAQ and the net contributions of processes calculated above can be achieved. Besides the nc file generated in Step I, the definition of targeted region grids and borders (the grids within the targeted region and adjacent to the outside regions) should also be provided by the users. Any software with basic data analysis and nc-file processing (Python, MATLAB, R, etc.) functions can be applied for this step.

The calculation processes in this step include:

- Calculation of hourly contributions of horizontal transport to O_3 mass changes through each user-defined border (horizontal transport contributions in every interface between the border grids and the outside regions, in both x- and y-directions, are taken into the calculations).
- Calculation of hourly contributions of vertical exchange near the ABL top to O_3 mass changes as well as the contributions of other processes within user-defined targeted region grids.
- Calculation of the hourly O_3 concentration budget (the contributions of processes to the hourly variations of O_3 concentrations) based on transport contributions to O_3 mass changes and the corresponding volumes of transported air parcels.

More details on the calculation of the O_3 concentration budget are introduced as follows. As displayed in Fig. S1, within an hour, the mean O_3 concentration within the ABL of the targeted region changes from c_0 to c_1. Normally, O_3 mass and ABL volume both change notably, making it difficult to quantify the contributions to O_3 concentration variations by various processes. It should be noted that this is also one of the main reasons why the regional O_3 mass and concentration budgets are different. To simplify the calculation, two calculation paths (shown as the red arrow lines in Fig. S1; c_{r1} and c_{r2} are the reference O_3 concentrations separately for two calculation paths) are used in the calculations, assuming that only O_3 mass or ABL volume change in each step of two paths. For the path "c_0 => c_{r1} => c_1", the first step is the ABL volume change step, with O_3 concentration change described as:

$$c_{r1} - c_0 = c_0 \times \left(\frac{\sum H_0}{\sum H_1} - 1\right) \tag{S1}$$

where H_0 and H_1 are the ABL heights at the starting and end hours. It is counted as part of the contributions by ABLex-H. The second step is the O_3 mass change step, with O_3 concentration change described as:

$$\begin{aligned} c_1 - c_{r1} = {} & \frac{\sum(F_{htrans} - c_{r1} \times \Delta V_{htrans})}{L^2 \times \sum H_1} + \frac{\sum(F_{ABLex-M} - c_{r1} \times \Delta V_{ABLex-M})}{L^2 \times \sum H_1} + \frac{F_{ABLex-H}}{L^2 \times \sum H_1} \\ & + \frac{F_{chem}}{L^2 \times \sum H_1} + \frac{F_{cloud}}{L^2 \times \sum H_1} + \frac{F_{ddep}}{L^2 \times \sum H_1} \end{aligned} \tag{S2}$$

where F_{htrans}, $F_{ABLex-M}$, $F_{ABLex-H}$, F_{chem}, F_{cloud} and F_{ddep} indicate the contributions of horizontal transport, ABLex-M, ABLex-H, gas-phase chemistry, cloud process and dry deposition, respectively, to O_3 mass changes. ΔV_{htrans} and $\Delta V_{ABLex-M}$ are the volumes of transported air parcels attributed to horizontal transport and ABLex-M, respectively, within an hour. L denotes the length of the grid cell, or the horizontal resolution of the model. The six terms on the right-hand side of the above formula are separately classified as the individual contribution of horizontal transport, ABLex-M, ABLex-H, gas-phase chemistry, cloud process and dry deposition in the O_3 concentration budgets. Note that the contributions of ABLex-H are separately calculated in two steps. Similarly, for the path "c_0 => c_{r2} => c_1", the changes in O_3 concentration in two steps can be described as:

$$\begin{aligned} c_{r2} - c_0 = {} & \frac{\sum(F_{htrans} - c_0 \times \Delta V_{htrans})}{L^2 \times \sum H_0} + \frac{\sum(F_{ABLex-M} - c_0 \times \Delta V_{ABLex-M})}{L^2 \times \sum H_0} + \frac{F_{ABLex-H}}{L^2 \times \sum H_0} \\ & + \frac{F_{chem}}{L^2 \times \sum H_0} + \frac{F_{cloud}}{L^2 \times \sum H_0} + \frac{F_{ddep}}{L^2 \times \sum H_0} \end{aligned} \tag{S3}$$

$$c_1 - c_{r2} = c_{r2} \times \left(\frac{\sum H_0}{\sum H_1} - 1\right) \tag{S4}$$

The contributions of various processes can be classified correspondingly. The final results of contributions by processes are the average values of these calculated based on two calculation paths.

Text S2. Comparisons of the O_3 concentration budget calculations between this study and 1-D models

When the region column in the Chemical Transport Models (CTMs) is thin enough to resemble a line, the O_3 concentration budget calculations using the CTMs results are expected to be the same as those in 1-D models. Thus, we can use it to check the validity of the O_3 concentration budget calculations in this study.

Here the contributions of horizontal transport to the variations of O_3 concentration over the studied space ($\langle c \rangle$) can be described as (Eq. (6) in the manuscript):

$$\left[\frac{\partial \langle c \rangle}{\partial t}\right]_{htrans} = \frac{F_{htrans} + \langle c \rangle (V - dV)}{V} - \langle c \rangle = \frac{F_{htrans} - \langle c \rangle dV}{V} \tag{S5}$$

where F_{htrans} is the contributions of horizontal transport to O_3 mass changes; V is the original volume of the PRD grids below the ABL; $dV$is the volume of transported parcels. Assume that the length of the region in the x-directions is *dx*, thus,

$$V = S\,dx \tag{S6}$$

where S is the area of the interface. As calculated in the O_3 mass budget, in the unit time,

$$F_{htrans} = cuS \tag{S7}$$

$$dV = uS \tag{S8}$$

where c is the O_3 concentration in the transported air parcels, and u is the mean horizontal wind speed in the interface. Therefore, from Eqs. (S5)-(S8), we can get:

$$\left[\frac{\partial \langle c \rangle}{\partial t}\right]_{htrans} = u\frac{\mathrm{c} - \langle c \rangle}{dx} = u\frac{dc}{dx} \tag{S9}$$

For ABLex-H, its contributions when V is much higher than dV (this assumption can be normally met when the period is short) are:

$$\left[\frac{\partial \langle c \rangle}{\partial t}\right]_{ABLex-H} = \frac{F_{ABLex-H} + \langle c \rangle V}{V + dV} - \langle c \rangle \approx \frac{F_{ABLex-H} - \langle c \rangle dV}{V} \tag{S10}$$

where $F_{ABLex-H}$ is the O_3 mass change attributed to ABLex-H. In the unit time,

$$F_{ABLex-H} = c_h \frac{\partial H}{\partial t} L^2 \tag{S11}$$

$$dV = \frac{\partial H}{\partial t} L^2 \tag{S12}$$

$$V = HL^2 \tag{S13}$$

where c_h is the O_3 concentration in the ABL top; L is the width of the grid cell (equal to the horizontal resolution of the model); H is the ABL height. Therefore, from Eqs. (S10)-(S13),

$$\left[\frac{\partial \langle c \rangle}{\partial t}\right]_{ABLex-H} = \frac{c_h - \langle c \rangle}{H}\frac{\partial H}{\partial t} \tag{S14}$$

For ABLex-M,

$$\left[\frac{\partial\langle c\rangle}{\partial t}\right]_{ABLex-M} = \frac{F_{ABLex-M} + \langle c\rangle(V - dV)}{V} - \langle c\rangle = \frac{F_{ABLex-M} - \langle c\rangle dV}{V} \tag{S15}$$

$F_{ABLex-M}$ is the O_3 flux attributed to ABL-FT-M. In the unit time,

$$F_{ABLex-M} = c_h\left(u_h\frac{\partial H}{\partial x} + v_h\frac{\partial H}{\partial y} - w_h\right)L^2 \tag{S16}$$

$$dV = \left(u_h\frac{\partial H}{\partial x} + v_h\frac{\partial H}{\partial y} - w_h\right)L^2 \tag{S17}$$

$$V = HL^2 \tag{S18}$$

where u_h, v_h and w_h are the ABL-top wind speeds in the x, y and z-direction, respectively. Therefore, from Eq. (S15-18),

$$\left[\frac{\partial\langle c\rangle}{\partial t}\right]_{ABLex-M} = \frac{c_h - \langle c\rangle}{H}\left(u_h\frac{\partial H}{\partial x} + v_h\frac{\partial H}{\partial y} - w_h\right) \tag{S19}$$

$$\begin{aligned}\left[\frac{\partial\langle c\rangle}{\partial t}\right]_{ABLex} &= \left[\frac{\partial\langle c\rangle}{\partial t}\right]_{ABLex-H} + \left[\frac{\partial\langle c\rangle}{\partial t}\right]_{ABLex-M} = \frac{c_h - \langle c\rangle}{H}\left(\frac{\partial H}{\partial t} + u_h\frac{\partial H}{\partial x} + v_h\frac{\partial H}{\partial y} - w_h\right)\\ &= \frac{w_e\Delta c}{H}\end{aligned} \tag{S20}$$

where w_e is the entrainment rate of the ABL; Δc is equal to the difference between O_3 concentrations above and within the ABL. Therefore, for these transport processes, the above formulas (Eqs. (S9), (S14), (S19), and (S20)) are the same as those used in 1-D models (Janssen and Pozzer, 2015; Vilà-Guerau de Arellano et al., 2015), suggesting their applicability in the quantification of the O_3 concentration budget using CTMs modelling results.

Text S3. Model validation of ABL height, wind and O_3 mixing ratio profiles based on the IAGOS dataset

IAGOS (In-service Aircraft of a Global Observing System; https://www.iagos.org) is a global aircraft-based observing system, where state-of-the-art instruments deployed in aircraft are used to measure reactive gases, greenhouse gases, aerosol and clouds in the troposphere and lower stratosphere (Petzold et al., 2016). Meteorological parameters, including air temperature, wind speed and direction, are also provided by IAGOS. When the aircraft climb up or descend, these measurements are suitable for obtaining the vertical profiles of parameters with high resolutions, which provides valuable observational datasets for the model validation in the vertical direction.

To ensure reasonable quantifications of the O_3 budgets, the IAGOS dataset in two representative months in Hong Kong (located in the south PRD) was used to evaluate the modelling performance of WRF-CMAQ in this study. We focused on comparing parameters within the height range of 0-5 km. Since observational data is often missing in some height ranges and the vertical resolution of modelling results is relatively low, we calculated the mean observational and modelling values within every 500 m height range (i.e., 0-500 m, 500-1000 m, etc.) for the comparisons. The detailed evaluations are introduced as follows:

(1) Atmospheric boundary layer (ABL) heights:

ABL heights are used to quantify the contribution of vertical exchange near the ABL top in the O_3 budgets. Therefore, the evaluation of modelled ABL heights is important. In this study, the observational ABL heights were determined using the profiles of potential temperature (θ) in IAGOS, defined as the heights where the lapse rate of θ ($\partial\theta/\partial z$, the rate of θ changing over height change) reaches its maximum values (Dai et al., 2014). Since there are limited profiles available in July 2016 and night-time ABL heights are hard to determine accurately, we only evaluated the modelling performance of ABL heights during the daytime (6:00-18:00 Local Time (LT)) of Oct. 2015. As shown in Fig. S10, the mean bias (MB) between modelling and observational ABL heights in Hong Kong is only -1.1 m, and a good correlation between ABL heights from two datasets (R = 0.76) suggests that the mean diurnal cycles of ABL can be modelled well. Though the modelling performance of ABL heights is satisfying based on the IAGOS dataset in Hong Kong, more comprehensive comparisons based on three-dimensional observations with higher spatiotemporal resolutions and coverages are required for more accurate O_3 budget estimates in future studies.

(2) Wind profiles:

Figure S5 shows the IAGOS and modelling wind roses within the height ranges of 0-1000 m, 1000-2000 m and 2000-5000 m. Both datasets indicate that higher wind speeds can be generally found at higher altitudes. In autumn, WRF overestimates wind speed below 1000 m by 0.6 m/s (16%) but underestimates it above 1000 m. In summer, the biases between wind speeds in the two datasets are relatively smaller, especially at lower heights (< 2000 m). Both datasets show similar prevailing wind

directions at different height ranges and seasons. Thus, the modelling performance of wind speeds and directions in the vertical direction is acceptable.

(3) O_3 mixing ratio profiles:

The comparisons between observational and modelling profiles of the O_3 mixing ratio are displayed in Fig. S7. Few O_3 profiles were available in July 2016, and the useable ones were mostly measured during clean periods. Thus, the comparison was mainly based on the results in Oct. 2015 (the number of IAGOS O_3 profiles available for the comparisons is 41). Both datasets show that the O_3 mixing ratio decreases with height in Hong Kong. Below the height of 1000 m, the observational and modelling O_3 mixing ratios are 71.4 ppbv and 75.8 ppbv, respectively. Within the height range of 1000-2000 m, the O_3 mixing ratio is overestimated by 26%. High O_3 levels during Oct. 13-24 and relatively low O_3 levels in other periods can be found in both datasets, suggesting that the developments of O_3 pollution in the month were modelled well. Therefore, the performance of O_3 profile modelling can also meet the requirement of O_3 budget calculations.

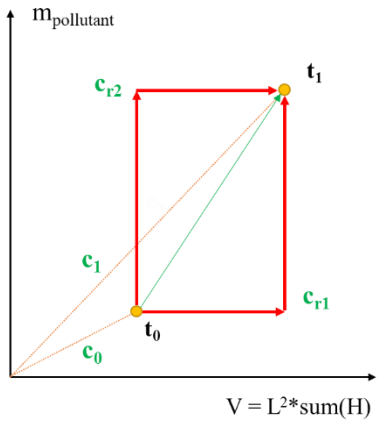

Figure S1. Two calculation paths for the regional O_3 concentration budget within an hour. $m_{pollutant}$ indicates the total mass of pollutants in the atmospheric boundary layer (ABL) of the studied region; V is the volume of the ABL of the region; L is the length of the grids (equal to the horizontal resolution of the model); H is the ABL heights; t_0 and t_1 are the starting and end hours; c_0 and c_1 are the concentrations of pollutants in t_0 and t_1, respectively; c_{r1} and c_{r2} are the reference concentrations of pollutants for two calculation paths.

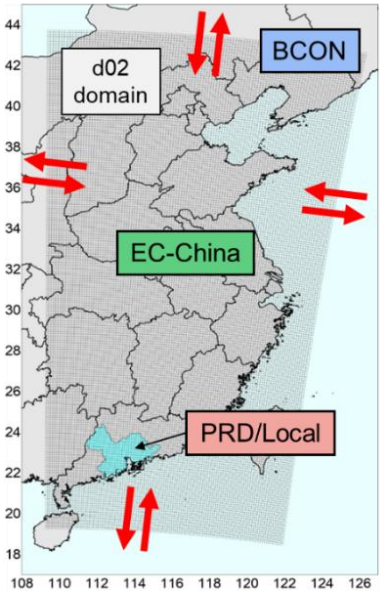

Figure S2. The spatial distributions of the d02 modelling domain and source regions. PRD, Pearl River Delta; EC-China, East and Central China; BCON, the boundary conditions of d02 modelling, or the contributions of sources outside d02.

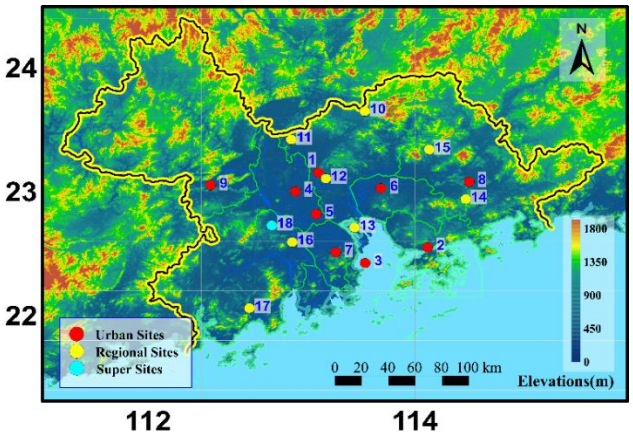

Figure S3. Spatial distributions of 18 sites of the Guangdong-Hong Kong-Macao Pearl River Delta Regional Air Quality Monitoring Network. The names of all sites and their located municipalities are: 1. Luhu, Guangzhou; 2. Liyuan, Shenzhen; 3. Tangjia, Zhuhai; 4. Huijingcheng, Foshan; 5. Jinjuju, Foshan; 6. Nanchengyuanling, Dongguan; 7. Zimaling, Zhongshan; 8. Xiapu, Huizhou; 9. Chengzhongzizhan, Zhaoqing; 10. Tianhu, Guangzhou; 11. Zhudong, Guangzhou; 12. Modiesha, Guangzhou; 13. Wanqingsha, Guangzhou; 14. Jinguowan, Huizhou; 15. Xijiao, Huizhou; 16. Donghu, Jiangmen; 17. Duanfen, Jiangmen; 18. Heshan Supersite, Jiangmen.

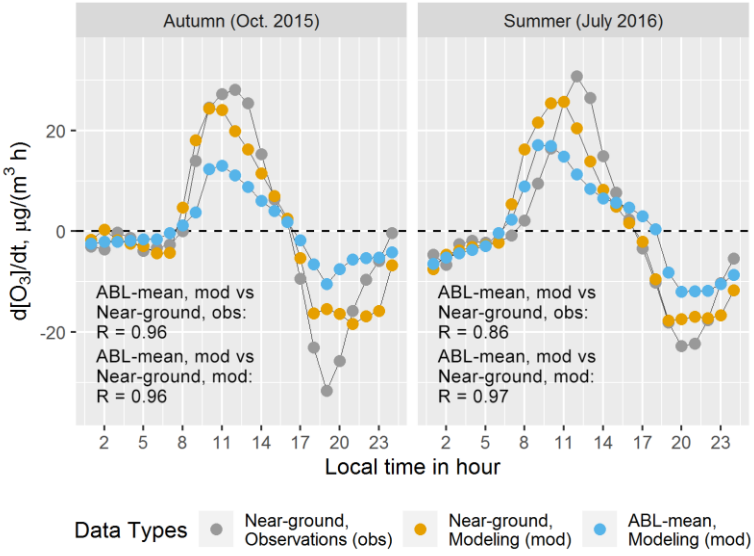

Figure S4. Mean diurnal change of the hourly variations of observational, modelling mean near-ground O_3 concentrations in 18 sites of the Guangdong-Hong Kong-Macao regional monitoring network and modelling mean O_3 concentration over the atmospheric boundary layer (ABL) of the Pearl River Delta on the polluted days of autumn (Oct. 2015) and summer (July 2016).

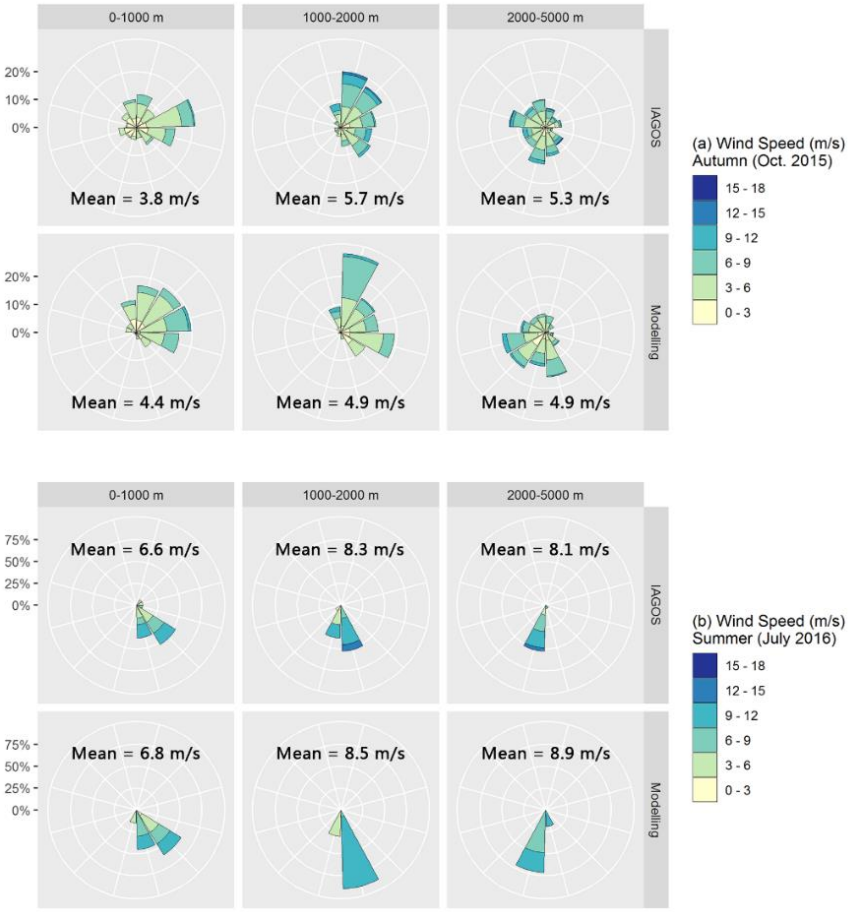

Figure S5. Comparisons between IAGOS and modelling wind roses in Hong Kong in (a) Oct. 2015 and (b) July 2016. Results within the height range of 0-1000 m, 1000-2000 m, and 2000-5000 m were separately displayed.

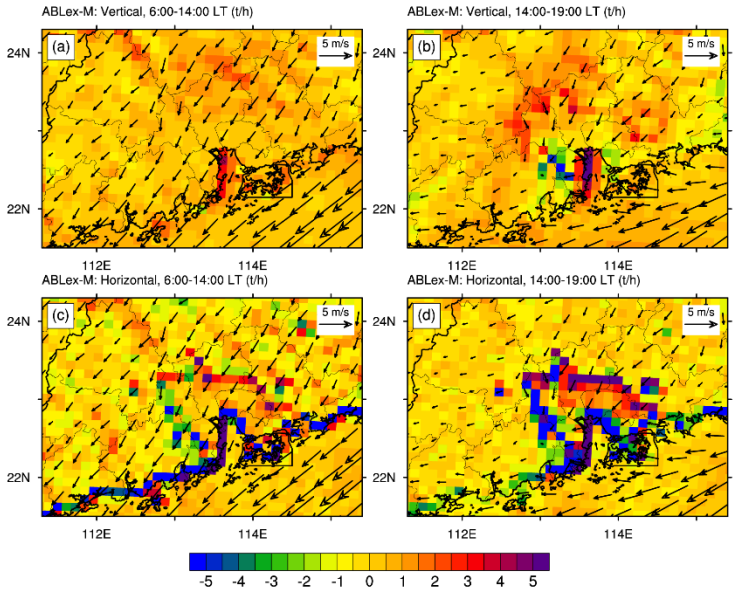

Figure S6. The spatial distributions of contributions of ABLex-M to O_3 mass changes on the polluted days of Oct. 2015. (a-b) Contributions through vertical advection; (c-d) contributions through horizontal advection. (a,c) The mean results during the morning hours (6:00-14:00 LT); (b,d) the mean results during the afternoon hours (14:00-19:00 LT).

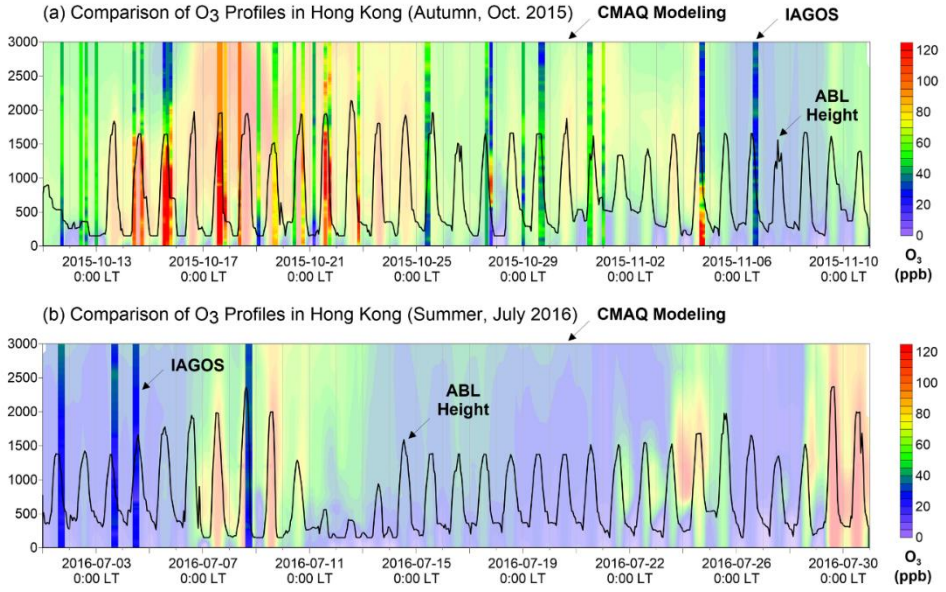

Figure S7. Comparisons between IAGOS and CMAQ modelling vertical profiles of O_3 mixing ratios (ppb) in Hong Kong in (a) Oct. 2015 and (b) July 2016. The heights of the atmospheric boundary layer (ABL) modelled by WRF in two months are also shown as solid black lines.

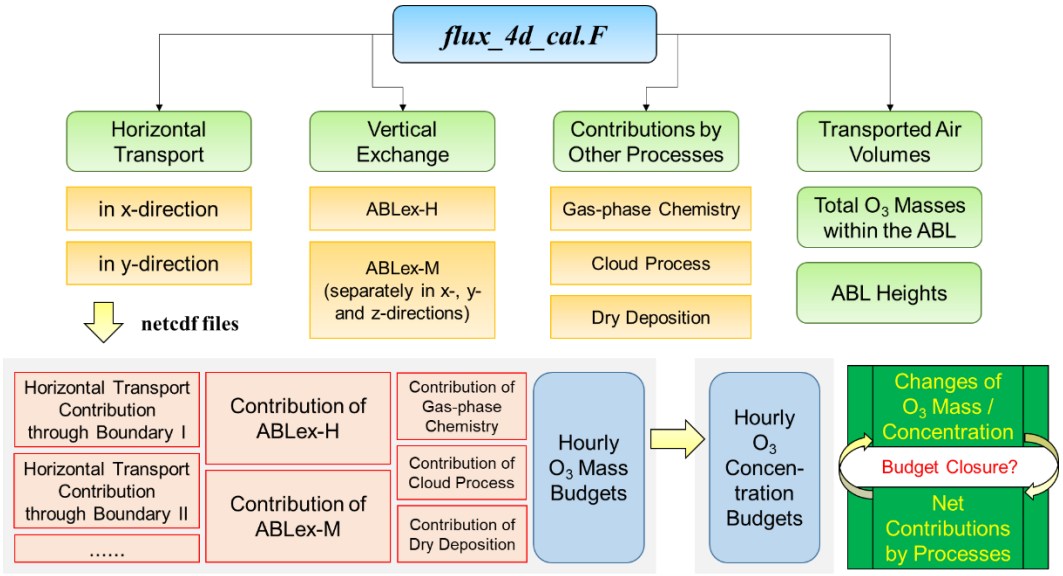

Figure S8. Flow diagram of the O_3 budget calculation processes. ABL, atmospheric boundary layer; ABLex-H, vertical exchange near the ABL top due to the changes of ABL height; ABLex-M, vertical exchange near the ABL top due to the large-scale air motions (advection through the ABL top).

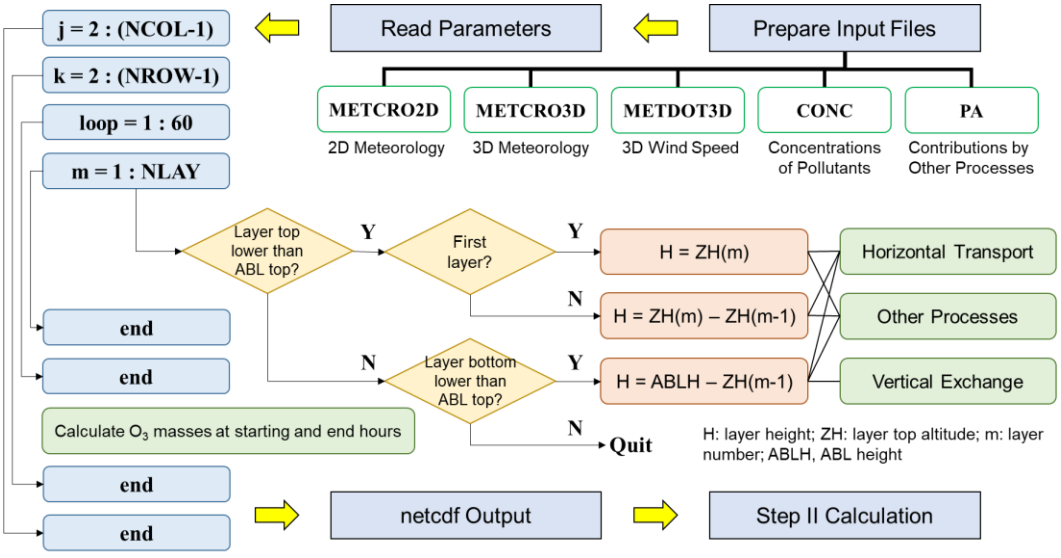

Figure S9. Flow diagram of the O_3 budget calculation in Step I (or the post-processing tool *flux_4d_cal*). NCOL, NROW and NLAY indicate the number of columns, rows and vertical layers in the modelling domain. ABL, atmospheric boundary layer. METCRO2D, 2-dimensional meteorological outputs from the MCIP module in CMAQ; METCRO3D, 3-dimensional meteorological outputs from the MCIP module in CMAQ; METDOT3D, 3-dimensional wind fields outputs from the MCIP module in CMAQ; CONC, 3-dimensional outputs of pollutant concentrations from CMAQ; PA, 3-dimensional outputs of hourly contributions by three non-transport processes to O_3 from CMAQ.

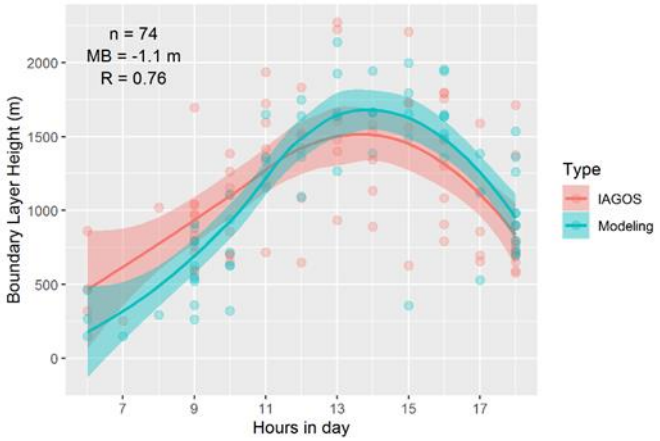

Figure S10. Comparisons between IAGOS and modelling atmospheric boundary layer height in Hong Kong in Oct. 2015. n, the number of the available dataset for the comparison; MB, mean bias; R, correlation factor.

Table S1. Information on the O_3 polluted days of the Pearl River Delta (PRD) in Oct. 2015 and July 2016. MDA1, the maximum 1-hr O_3 concentrations; MDA8, the maximum 8-hr average O_3 concentrations.

Dates	Influencing Weather Systems	O_3 concentrations in the PRD (the maximum values in nine municipals of the PRD, released by the China National Environmental Monitoring Centre; $\mu g/m^3$)	
		MDA1	MDA8
Oct.13, 2015	Typhoon Koppu and Champi	201	164
Oct.14, 2015		301	244
Oct.15, 2015		271	227
Oct.16, 2015		260	219
Oct.17, 2015		233	211
Oct.18, 2015		205	187
Oct.19, 2015		214	174
Oct.20, 2015		200	158
Oct.21, 2015		214	195
Oct.22, 2015		209	182
Oct.23, 2015		249	199
Oct.24, 2015		225	193
Oct.28, 2015	Subtropical High	238	186
Nov.3, 2015	Sea High	207	162
Nov.4, 2015		182	168
Nov.5, 2015		255	187
July 7, 2016	Typhoon Nepartak	297	256
July 8, 2016		260	198
July 9, 2016		263	231
July 10, 2016		211	150
July 22, 2016	Subtropical High	211	176
July 23, 2016		223	197
July 24, 2016		265	226
July 25, 2016		334	269
July 26, 2016		235	164
July 29, 2016		271	204
July 30, 2016	Typhoon Nida	268	187
July 31, 2016		385	344

Table S2. Formulas in the calculations of contributions to O_3 mass changes for the grid cell (i, j) in the unit time dt, parameters used and their source files in the *flux_4d_cal* tool.

Processes	Formulas of O_3 fluxes	Parameters used	Sources of parameters
Horizontal transport (in the x-direction)	$F_{u-trans} = \sum_{k=1}^{h} c_{i-1,j} u_{i,j+\frac{1}{2}} L \Delta z dt$	$c_{i-1,j}$: O_3 concentrations in the grid cell (i-1, j)	CONC files
		$u_{i,j+\frac{1}{2}}$: wind speeds in the west interface	METDOT3D files
		L: the length of grid cells (= model resolution)	User defined
		Δz: layer heights (H $- z_{h-1}$ for the ABL top layer, $z_k - z_{k-1}$ for other layers within the ABL; H, ABL height)	METCRO3D files
		h: the layer of ABL top	Determined by ABL height
Horizontal transport (in the y-direction)	$F_{v-trans} = \sum_{k=1}^{h} c_{i,j-1} v_{i+\frac{1}{2},j} L \Delta z dt$	$c_{i,j-1}$: O_3 concentrations in the grid cell (i, j-1)	CONC files
		$v_{i+\frac{1}{2},j}$: wind speeds in the south interface	METDOT3D files
		L: the length of grid cells (= model resolution)	User defined
		Δz: layer heights (H $- z_{h-1}$ for the ABL top layer, $z_k - z_{k-1}$ for other layers within the ABL; H, ABL height)	METCRO3D files
		h: the layer of ABL top	Determined by ABL height
ABLex-H	$F_{ABLex-H} = c_h \frac{\partial H}{\partial t} L^2 dt$	c_h: O_3 concentrations in the ABL top layer	CONC files
		$\frac{\partial H}{\partial t}$: the change rates of ABL height	METCRO2D files
		L: the length of grid cells (= model resolution)	User defined
ABLex-M (in the x-direction)	$F_{ABLex-Mx} = c_{i-1,j(h)} u_{i,j+\frac{1}{2}(h)} \frac{\partial H}{\partial x} L^2 dt$	$c_{i-1,j(h)}$: O_3 concentrations in the ABL top layer of the grid cell (i-1, j)	CONC files
		$u_{i,j+\frac{1}{2}(h)}$: wind speeds in the ABL top layer of the west interface	METDOT3D files
		L: the length of grid cells (= model resolution)	User defined
		$\frac{\partial H}{\partial x}$: the difference of ABL heights in x-direction, or between the grid cells (i, j) and (i-1, j)	METCRO2D files
ABLex-M (in the y-direction)	$F_{ABLex-My} = c_{i,j-1(h)} v_{i+\frac{1}{2},j(h)} \frac{\partial H}{\partial y} L^2 dt$	$c_{i,j-1(h)}$: O_3 concentrations in the ABL top layer of the grid cell (i, j-1)	CONC files
		$v_{i+\frac{1}{2},j(h)}$: wind speeds in the ABL top layer of the south interface	METDOT3D files
		L: the length of grid cells (= model resolution)	User defined
		$\frac{\partial H}{\partial y}$: the difference of ABL heights in y-direction, or between the grid cells (i, j) and (i, j-1)	METCRO2D files
ABLex-M (in the z-direction)	$F_{ABLex-Mz} = -c_h w_h L^2 dt$	c_h: O_3 concentrations in the ABL top layer	CONC files
		w_h: vertical wind speeds in the ABL top layer	METCRO3D files
		L: the length of grid cells (= model resolution)	User defined
Other processes (gas-phase chemistry, cloud process, dry deposition)	$F_{others} = \sum_{k=1}^{h} IPR \Delta z dt$	IPR: integrated process rates of pre-set processes	PA files
		Δz: layer heights (H $- z_{h-1}$ for the ABL top layer, $z_k - z_{k-1}$ for other layers within the ABL; H, ABL height)	METCRO3D files
		h: the layer of ABL top	Determined by ABL height

References (of the Supplement)

Chan, R. L. M., Lee, O. S. M., and Cheng, A. Y. S.: Diurnal variation of mixing height in Hong Kong. In Reviewed and revised papers presented at the 23rd International Laser Radar Conference (pp. 737-740), 2006.

Dai, C., Wang, Q., Kalogiros, J. A., Lenschow, D. H., Gao, Z., and Zhou, M.: Determining Boundary-Layer Height from Aircraft Measurements, Bound.-Lay. Meteorol., 152, 277–302, https://10.1007/s10546-014-9929-z, 2014.

Fan, S. J., Fan, Q., Yu, W., Luo, X. Y., Wang, B. M., Song, L. L., and Leong, K. L.: Atmospheric boundary layer characteristics over the Pearl River Delta, China, during the summer of 2006: measurement and model results, Atmos. Chem. Phys., 11, 6297–6310, https://doi.org/10.5194/acp-11-6297-2011, 2011.

He, G., Deng, T., Wu, D., Wu, C., Huang, X., Li, Z., Yin, C., Zou, Y., Song, L., Ouyang, S., Tao, L., and Zhang, X.: Characteristics of boundary layer ozone and its effect on surface ozone concentration in Shenzhen, China: A case study, Sci. Total Environ., 791, 148044, https://doi.org/10.1016/j.scitotenv.2021.148044, 2021.

Janssen, R. H. H. and Pozzer, A.: Description and implementation of a MiXed Layer model (MXL, v1.0) for the dynamics of the atmospheric boundary layer in the Modular Earth Submodel System (MESSy), Geosci. Model Dev., 8, 453–471, https://doi.org/10.5194/gmd-8-453-2015, 2015.

Petzold, A., Thouret, V., Gerbig, C., Zahn, A., Brenninkmeijer, C. A. M., Gallagher, M., Hermann, M., Pontaud, M., Ziereis, H., Boulanger, D., Marshall, J., Nédélec, P., Smit, H. G. J., Friess, U., Flaud, J.-M., Wahner, A., Cammas, J.-P., Volz-Thomas, A. and IAGOS TEAM: Global-scale atmosphere monitoring by in-service aircraft–current achievements and future prospects of the European Research Infrastructure IAGOS, Tellus B, 67, 28452, https://doi.org/10.3402/tellusb.v67.28452, 2015.

Song, L., Deng, T., Li, Z. N., Wu, C., He, G. W., Li, F., Wu, M., and Wu, D. (2021). Retrieval of boundary layer height and its influence on $PM_{2.5}$ concentration based on lidar observation over Guangzhou, J. Trop. Meteorol., 27(3), 303-318, https://doi.org/10.46267/j.1006-8775.2021.027, 2021.

Vilà-Guerau De Arellano, J., van Heerwaarden, C. C., van Stratum, B. J. H., and van den Dries, K.: Atmospheric Boundary Layer: Integrating Air Chemistry and Land Interactions, Cambridge University Press, New York, 2015.